5

Photonics

Table of Contents

Deep Submicron CMOS Photonics

J.S. Orcutt, A. Khilo, M.A. Popović, C.W. Holzwarth, B. Moss, H. Li, M.S. Dahlem, F.X. Kärtner, E.P. Ippen, J.L. Hoyt, V. Stojanović, R.J. Ram

Sponsorship: DARPA

In the past decade, silicon has moved from a work bench for low-index contrast photonics to a strong-confinement (SC) photonics workhorse. The SC silicon-core waveguides have been shown to maintain low-loss while enabling micron-scale photonic structures [1] and suitability for next-generation telecom components [2]. As performance begins to rival traditional III-V telecom-grade photonics, the possibility of inter- and intrachip photonic interconnects integrated with traditional CMOS electronics has opened photonics to the VLSI community [3]. Photonic interconnects have the potential to break increasingly severe energy efficiency and bandwidth density bottlenecks of electrical interconnect in scaled CMOS microprocessors. Photonic components required for integration include SC waveguides, resonant add-drop filters for wavelength-division multiplexing (WDM), energy-efficient modulators, and integrated photodiodes. In this work, we present a general strategy for photonic integration into bulk CMOS and the first photonic test chip using this approach, which was produced in a commercial 65-nm process and is shown in Figure 1(a).

Traditional silicon-on-insulator (SOI) waveguides that use the active electronic silicon layer of SOI wafers as the waveguide core require a thick buried-oxide layer (2 to 3 μm) to enable low optical substrate leakage loss. The photonic chip presented here is produced within an existing commercial bulk CMOS flow, adding zero in-house production changes, ensuring optimal performance of integrated electronic circuits and minimizing production cost. Bulk CMOS processes, unlike SOI CMOS, have no single-crystal silicon layer patternable with a standard mask set. Multiple higher index nitride layers that could potentially be used as waveguide cores are present in the backend of the CMOS processes, but none are patternable. However, a patternable polysilicon layer in the front end of the process, referred to as a shallow trench isolation (STI), is used to form the transistor gates over a thin oxide as well as local interconnects and resistors over a thicker oxide. Traditionally, the end of line polysilicon is heavily doped and silicided to reduce electrical resistance, resulting in a material with high optical loss. However, this Si layer must first be deposited undoped since opposite polarity implant steps are used to form the n-channel and p-channel transistor gates. Additionally, the need to create accurate resistors in a mixed-signal process requires a way to block the standard silicidation step of the polysilicon. These two facts allow for the processing masks to be designed to create an undoped, unsilicided polysilicon layer for SC waveguide fabrication.

Using this platform, we designed the first bulk photonic chip in a commercial process on a 4-mm² die. Primary goals are for the chip to demonstrate integrability, characterize waveguide loss and evaluate the performance of the photonic device. Additionally, the chip includes high-speed modulator drivers with data input signal processing electronics that are designed to demonstrate integration with photonics without degrading the performance of the electronic device.

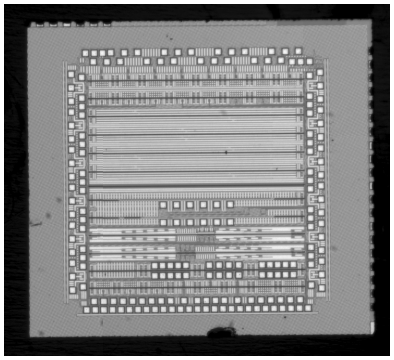

▲ Figure 1: Bulk 65-nm photonic test chip die photo. The 2x2 mm² die contains 116 devices and over 21 cm of waveguide.

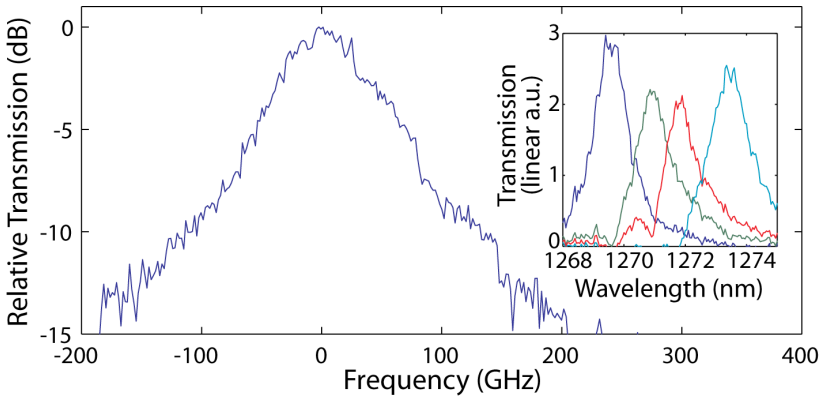

▲ Figure 2: Single channel microring-resonator drop port results. Inset shows a 4-channel filter bank with 240-GHz channel spacing (preliminary measurements taken by IR camera show some distortion due to pixel saturation and limited bit depth).

References

[1] F. Xia et al., "Ultracompact optical buffers of a silicon chip," *Nature Photonics*, vol. 1, no. 1, pp. 65-71, Jan. 2007.

[2] M.A. Popović, T. Barwicz, et al., "Strong-confinement microring resonator photonic circuits," in *Proc. 20th Annual Meetingof IEEE Lasers and Electro-Optics Society*, Lake Buena Vista, Florida, Oct. 2007, paper TuCC3.

[3] C. Gunn, "Fully integrated VLSI CMOS and photonics CMOS photonics," in *Digest of Technical Papers, IEEE Symposium on VLSI Technology*, 2007, pp. 6-9.

Active Control of Photonic Microring Filters

R. Amatya, R.J. Ram
Sponsorship: DARPA

Microring resonators can be used as pass-band filters for wavelength-division demultiplexing in electronic-photonic integrated circuits for applications such as analog-to-digital converters. For high-quality signal transmission, the resonant frequency of the filter must be held at a certain value to allow minimum timing errors in the sampling of the signal. Thermal tuning is used to compensate for any fabrication errors or environmental temperature fluctuations that might lead to a shift in the resonant frequency. With an optimized heater design (Figure 1), we demonstrate efficient thermal tuning with low power (80μW/GHz) for these ring resonators. For the application of interest, wavelength stability as well as power efficiency for tuning are more important metrics than the total tuning range. A distinct disadvantage of working with silicon is the stringent need for temperature stability. Due to the larger thermo-optic coefficient of silicon, the resonant wavelength is very susceptible to temperature change.

An on-chip heater is run by a temperature controller feedback circuit, which helps in maintaining a steady temperature against environmental temperature perturbations. Due to size constraints for microring resonators (radius ~ 10 μm), a single resistive element is used both as a heater and as a temperature sensor. The feedback circuit utilizing a proportional-integral-derivative (PID) controller tries to maintain the overall balance between the voltages of the heater and the set resistor such that the error in the voltage difference measured by an instrumentation amplifier is least.

To show the thermal stability of the system, an experiment was conducted in which an external temperature perturbation was introduced by shining a white light source on the sample. When the light is on, a temperature variation of 1 K is introduced to the filter chip. With the closed-loop feedback, the temperature variation is reduced to an average fluctuation of 80 mK, which is equivalent to the frequency variation of 280 MHz (Figure 2). The speed of the feedback circuit to compensate for the temperature perturbation is on the order of a few tens of milliseconds.

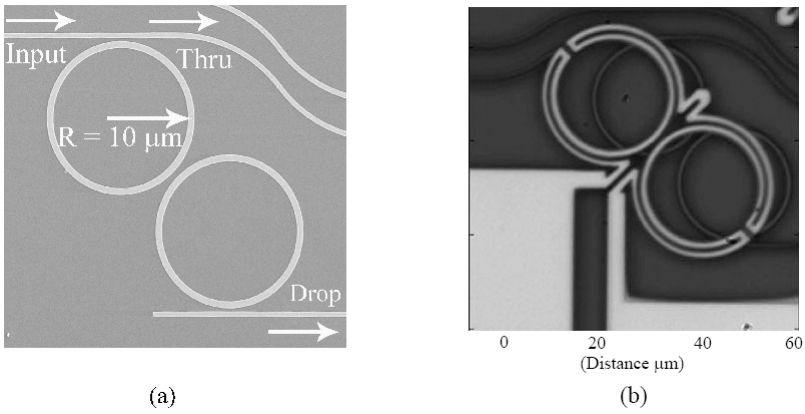

▲ Figure 1: An SEM picture of the microring heater on top of the filter.

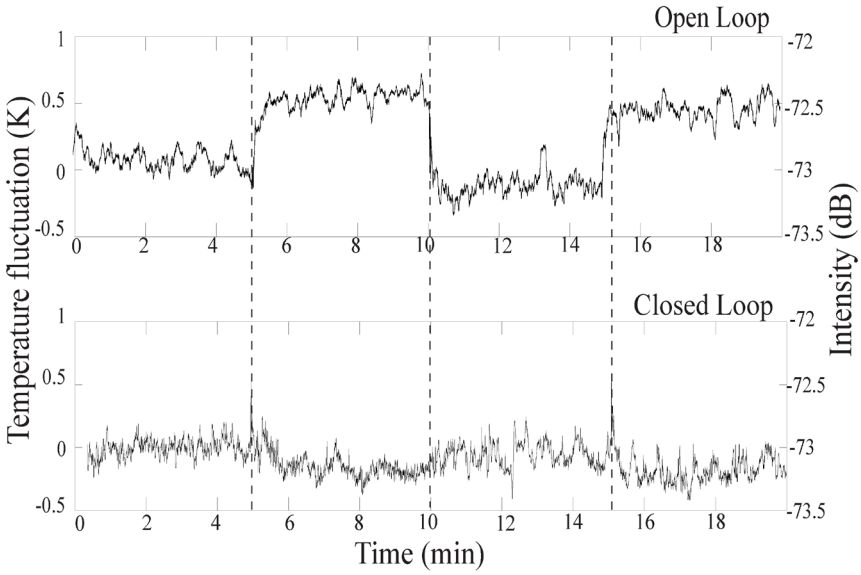

▲ Figure 2: Thermal control achieved within 80 mK of the absolute value for the second-order ring resonator using feedback control loop.

Nanofabrication of Hitless Reconfigurable Optical Add-drop Multiplexers Based on Silicon Microrings

C.W. Holzwarth, T. Barwicz, M.A. Popovic, P.T. Rakich, M. Dahlem, F. Gan, E.P. Ippen, F.X. Kaertner, H.I. Smith
Sponsorship: DARPA, internal funds

Reconfigurable optical add-drop multiplexers (ROADMs) are key components of modern optical networks. Data in optical fibers is carried at numerous wavelengths, each defining a specific "channel." The ROADMs allow the rerouting ("droping") of a subset of the data channels traveling in an optical fiber, replacing these with new data streams ("adding") at the previously rerouted wavelengths. The term "reconfigurable" indicates that the subset of dropped channels can be changed "on the fly," i.e., while the ROADM is in operation. For a ROADM to be truly useful in an optical network it must be "hitless," that is, it must enable tuning from one channel to a second channel without affecting the data transmitted on any of the other channels.

In our previous work, we developed precision nanofabrication techniques that enabled us to demonstrate the most advanced microring filters reported to date in silicon-rich silicon nitride [1,2]. In the present work, we employed silicon microrings to take advantage of their lower optical loss and higher thermo-optic coefficient, allowing wide tuning of the operating wavelengths of the ROADM via integrated heaters. Figure 1 presents a cross-sectional diagram and top-view micrograph of our implementation of a silicon waveguide and a hitless ROADM with integrated microheaters. Line-edge roughness is of critical concern in silicon waveguides as it translates into significant propagation loss via scattering of the guided mode. We found that the smoothest waveguides were obtained using hydrogen silsesquioxane (HSQ) as an e-beam resist and an etch-mask for the subsequent HBr-based reactive-ion etching. Figure 2 presents a scanning-electron micrograph of a coupling region between a microring and a bus waveguide defined in HSQ. The patterning is based on scanning-electron-beam lithography.

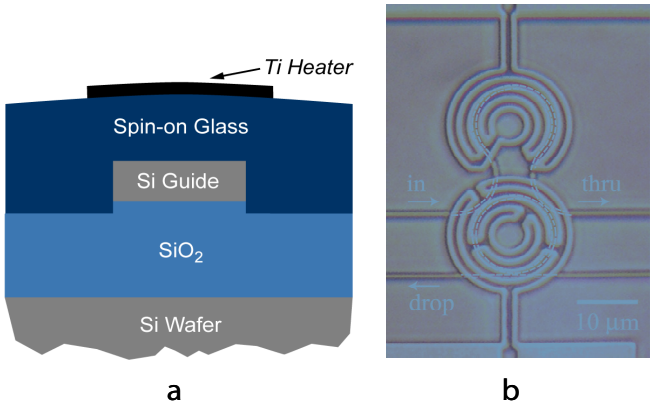

▲ Figure 1: (a) Cross-sectional schematic of a silicon waveguide with an integrated titanium heater. Spin-on glass is used for the upper cladding of the waveguide to allow self-planarization and to avoid filling problems in narrow gaps. (b) Top-view optical micrograph of the silicon-microring hitless ROADM with titanium microheaters.

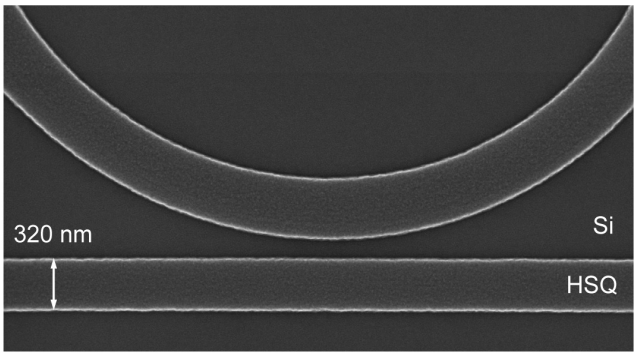

▲ Figure 2: Top-view scanning-electron micrograph of a coupling region defined in HSQ. The patterning is done with scanning-electron-beam lithography. The minimum feature size required (e.g., the gap) is ~100 nm and must be controlled to ~ 5 nm.

References

[1] M.A. Popovic, T. Barwicz, M.R. Watts, P.T. Rakich, L. Socci, E.P. Ippen, F.X. Kaertner, and H.I. Smith, "Multistage high-order microring-resonator add-drop filters," *Optics Letters*, to be published.

[2] T. Barwicz, M.R. Watts, M.A. Popovic, P.T. Rakich, E.P. Ippen, F.X. Kaertner, and H.I. Smith, "Polarization-insensitive optical add-drop multiplexers in silicon nitride," Massachusetts Institute of Technology, Cambridge, MA, Microsystems Technology Laboratories Annual Research Report, 2008.

Localized Substrate-Removal Technique Enabling Optical Intrachip Communication in Bulk-Silicon CMOS

C.W. Holzwarth, J.S. Orcutt, J. Sun, H. Li, M.A. Popovic, V. Stojanović, J.L. Hoyt, R.J. Ram, H.I. Smith
Sponsorship: DARPA

Efforts elsewhere to integrate photonics with CMOS electronics requires customization of the fabrication process to provide low-loss in the photonic components [1]. This compromises electronic performance, throughput, and cost. Customizations include thick low-index cladding layers, silicon-on-insulator material and electron-beam lithography. While tolerable for some applications, such customization is considered unacceptable for microprocessors and DRAM, circuits that would benefit the most from optical intrachip communication. In order to integrate photonics with circuits produced in high volume, one must be able to work within the constraints of commercial bulk CMOS process flows by utilizing industry-standard material layers, thicknesses, processing steps and tools. Waveguides fabricated out of the polysilicon layer used for transistor gates and poly-resistors above the shallow-trench isolation (STI) layer would have a propagation loss of the order of 1000 dB/cm since the STI layer (<400 nm) is not thick enough to prevent the guided optical mode from "leaking" into the high-index Si substrate.

To overcome this problem, we have developed a novel post-processing technique using XeF_2 to locally remove the silicon underneath the STI layer, as shown in Figure 1. The creation of air tunnels under the polysilicon waveguides eliminates propagation loss due to leakage into the substrate, and minimizes impact on the electrical, thermal, and mechanical performance of the electronics. XeF_2 gas is used because it etches Si isotropically, can undercut large areas without stiction problems, and has a high silicon-to-oxide etch-rate selectivity (>1000:1). We have used this method to fabricate waveguides in polysilicon-on-oxide films (Figure 2). The propagation loss of these waveguides was measured to be ~10 dB/cm at 1550 nm. Most of this loss is attributed to material absorption and scattering from surface and sidewall roughness [2].

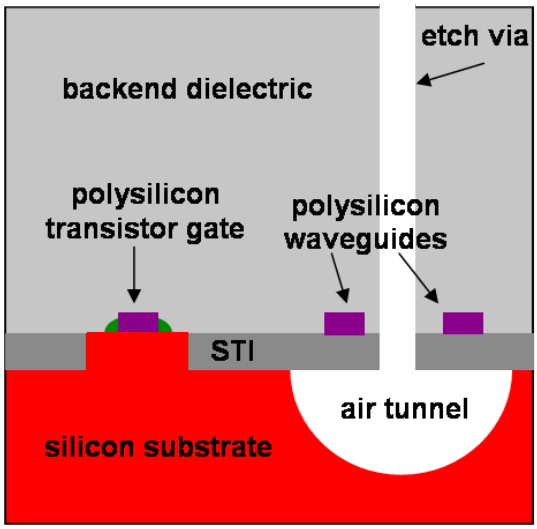

▲ Figure 1: Sketch of the cross-section of a bulk CMOS chip showing how electronics and photonic devices can be fabricated on the same chip with the addition of only a post-processing step to locally remove the silicon substrate beneath the polysilicon waveguides.

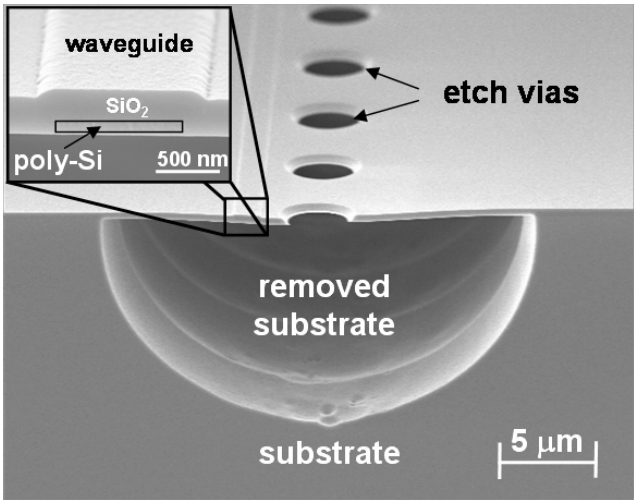

▲ Figure 2: Scanning-electron micrograph of fabricated poly-silicon waveguide using the XeF_2 based substrate removal technique. The inset shows a close-up of the waveguide. The SiO_2 cladding beneath the poly-silicon is only 50 nm thick, resulting in loss >1000 dB/cm before the localized substrate removal step. After removal, the loss is reduced to approximately 10 dB/cm.

References

[1] J.S. Orcutt et al., "Demonstration of the first electronic photonic integrated circuit in a commercial scale bulk CMOS Process," submitted to the *Conference of Lasers and Electro-Optics*, San Jose, California, May 2008.

[2] C.W. Holzwarth et al., "Localized Substrate Removal Technique Enabling Strong-Confinement Microphotonics in Bulk-Si CMOS Processes," submitted to the *Conference of Lasers and Electro-Optics*, San Jose, California, May 2008.

Nanofabrication of Optical Microring Filter Banks for Ultra-Fast Analog-to-Digital Converters

C.W. Holzwarth, T. Barwicz, M.A. Popović, A. Khilo, M. Dahlem, E.P. Ippen, F.X. Kärtner, H.I. Smith
Sponsorship: DARPA

Progress in designs and nanofabrication techniques for microring-resonators in high-index-contrast materials have made possible the wide spectral spacing between resonances and low loss required for electronic-photonic integrated circuits including ultra-fast analog-to-digital converters [1]. Achieving accurate resonant-frequency spacing of microring-filters is critical for these devices. In the NanoStructures Laboratory we have developed a technique using scanning-electron-beam lithography (SEBL) that is capable of accurately controlling the resonant frequency spacing in microring-resonator filter banks. The resonant wavelength of a microring-resonator filter is dependant on both the ring radius and the effective index of refraction of the ring waveguide. The effective index is controlled lithographically by controlling the width of the ring waveguide. Although it is simple to change both the width and the radius of the ring in the SEBL layout, this is limited to discrete jumps corresponding to the step size of the SEBL system. In order to have 1 GHz control of the resonant frequency for the designed filters the SEBL systems would need a step size of 30 pm. In our process this limitation of discrete step size is overcome by modulating the electron beam dose to precisely control the width of the ring waveguide [2].

In our experiment second-order microring-resonator filters, fabricated in silicon-rich silicon nitride and overcald with HSQ, were used in a microring filter banks (Figure 1a, 1b). Using dose modulation, twenty-channel dual-filter banks with a target channel spacing of 80 GHz were fabricated and tested, demonstrating control of changes in the average ring-waveguide width of 0.10 nm, despite the 6 nm SEBL step size (Figure 1c). Variations between filter responses were due to slight frequency mismatches between rings of the same filter, we demonstrated that this can be corrected by thermal trimming with integrated microheaters.

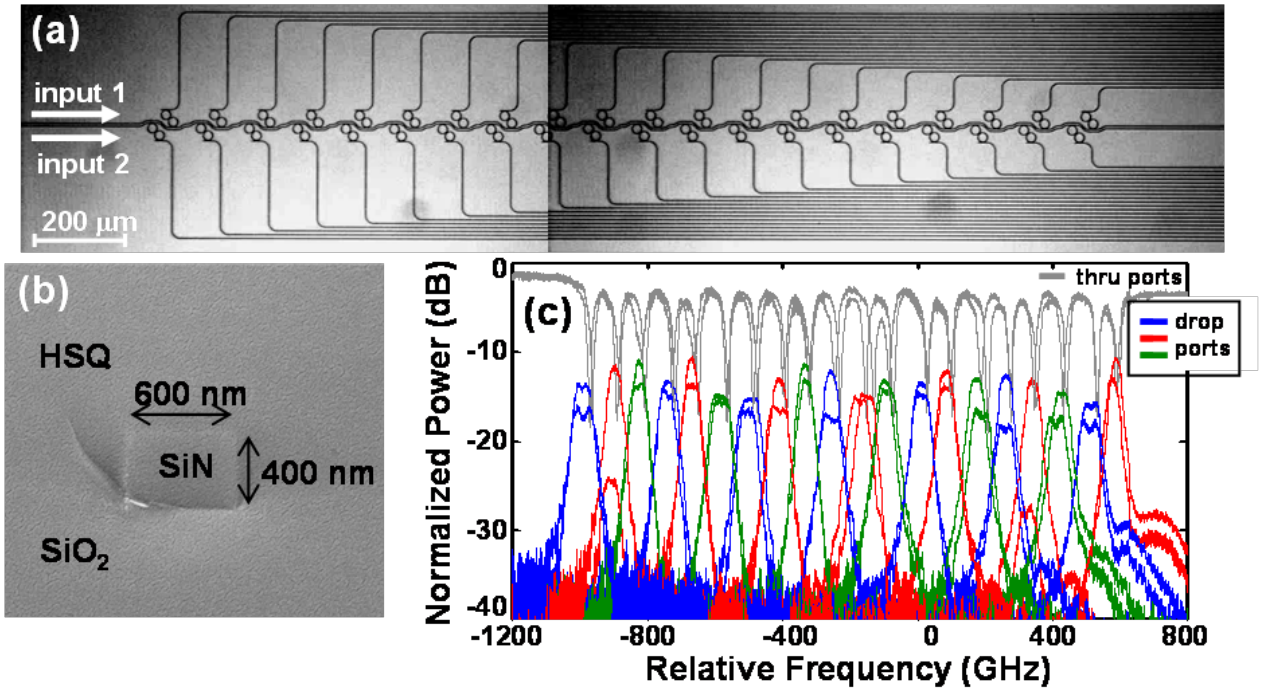

▲ Figure 1: a) Scanning-electron micrograph of fabricated second-order twenty-channel dual-filter bank and b) cross-section of overclad waveguide. c) Filter response of second-order twenty-channel dual-filter bank with an average channel spacing of 83 GHz.

References

[1] T. Barwicz, M.A. Popovic, P.T. Rakich, M.R. Watts, H.A. Haus, E.P. Ippen, and H.I. Smith, "Microring-resonator-based add-drop filters in SiN: fabrication and analysis," *Optics Express*, vol. 12, no. 7, pp. 1437-1442, Apr. 2004.

[2] C.W. Holzwarth, T. Barwicz, M. A. Popović, P. T. Rakich, F. X. Kaertner, E. P. Ippen, and H. I. Smith, "Accurate resonant frequency spacing of microring filters without postfabrication trimming," *Journal of Vacuum Science and Technology B*, vol. 24, no. 6, pp. 3244-3247, Nov. 2006.

Three-Dimensional Photonic Crystals in Si_3N_4 and Si by Assembly of Prepatterned Membranes

A.A. Patel, C. Fucetola, E.E. Moon, H.I. Smith
Sponsorship: NSF, DTRA

The diffraction of light within periodic structures (so-called "photonic crystals") offers a wide variety of opportunities for controlling and manipulating light. Most research to date has focused on 2-dimensional (2D) photonic crystals, because highly developed planar-fabrication techniques (i.e., lithography followed by pattern transfer) are directly applicable. However, the full potential of photonic crystals in futuristic sensing, communication and computation systems is best achieved with 3-dimensional (3D) structures. The problem is that new methods of 3D fabrication need to be developed to achieve desired complex structures over large areas with low cost and high yield.

Interference lithography can produce periodic 3D structures in photosensitive polymers, but the introduction of deviations from perfect periodicity (i.e., waveguides and structures that constitute "devices" within the periodic matrix, so-called "defects") is highly problematic. Moreover, it's not clear that backfilling 3D polymeric structures is applicable to a suitable range of materials. Layer-by-layer methods the use scanning-electron-beam lithography enable the controlled introduction of defects, but such fabrication is generally tedious, slow, low yield, and covers impractically small areas (e.g., <0.1mm on edge).

We describe a novel approach in which the 3D photonic-crystal structure is fabricated by assembling membranes that are patterned in advance using conventional planar methods (Figure 1). This approach minimizes the yield problem because membranes can be inspected and selected before assembly, and the desired waveguides and devices, can be introduced at any level in the assembly. When brought into contact, membranes that are free of particulate and other contamination will bond spontaneously by van der Waals or other mechanisms.

Previously we reported using low-stress Si_3N_4 membranes as the test vehicle. 2D periodic structures were etched into free-standing membranes, and nonaligned stacking carried out (Figure 2). Currently, we are addressing the lithographic challenge of patterning a large-area photonic structure in conjunction with custom alignment marks that will assist in gap detection and lateral overlay. In addition, we are developing a process for creating 3D photonic crystals in Si, using coherent-diffraction lithography and HBr reactive-ion etching. The Si membranes are obtained from SOI wafers.

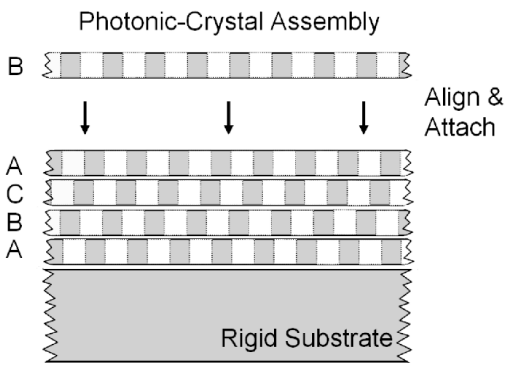

▲ Figure 1: Depiction of the layer-by-layer stacking approach to 3D photonic crystal fabrication. All the layers in the photonic crystal are fabricated in parallel. This reduces processing cycles, which will help improve yield and reduce lead times.

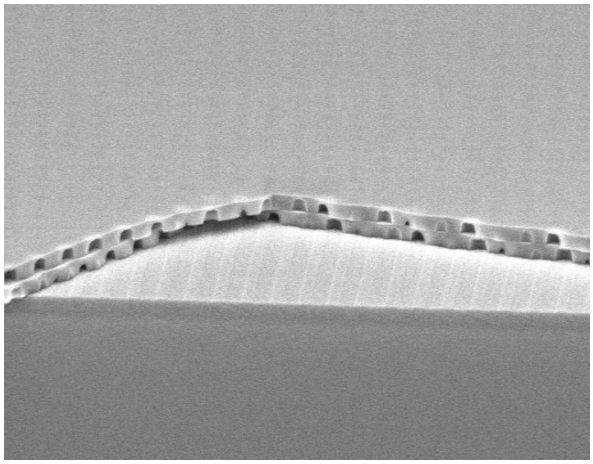

▲ Figure 2: Initial stacking experiment. A patterned SiN membrane is brought into contact with SiN substrate. The pitch of the array is 600nm and the membrane is 350nm thick. A second patterned membrane is brought into contact with the first.

Reference

[1] A.A. Patel and H.I. Smith, "Membrane stacking: A new approach for three-dimensional nanostructure fabrication," *Journal of Vacuum Science and Technology B*, vol. 26, no. 6, pp. 2662-2664, Nov. 2007.

Integrated HIC High-Q resonators in Chalcogenide Glass

J.J. Hu, N. Carlie, N.N. Feng, L. Petit, A. Agarwal, K. Richardson, L.C. Kimerling
Sponsorship: DOE

Optical resonance enhancement, combined with a significantly increased optical path length, makes ring resonators an ideal device platform for both fundamental investigations and practical applications based on photon-matter interactions. To date, most planar glass resonators have been fabricated with silica. Compared to silica, chalcogenide (ChG) glasses are superior material candidates for the aforementioned applications due to their unique optical properties in the infrared wavelengths. Of particular relevance here are the reduced phonon-quenching, the large Kerr optical non-linearity, and the wide infrared transparency window of ChG materials. We report the fabrication of integrated high-index-contrast (HIC) microring and microdisk resonators using a CMOS-compatible lift-off technique [1] in thermally evaporated As_2S_3 chalcogenide glass films. We demonstrate a new pulley-type configuration for optical coupling from photonic wire waveguides into these HIC micro-resonators with improved coupling efficiency. The WGM (whispering gallery mode) in micro-disk chalcogenide resonators exhibits a cavity Q as high as 205,000. Such a high Q-value represents a 20-fold improvement compared to chalcogenide glass photonic crystal resonators [2] and our recently demonstrated racetrack rings [3], and it is 2.5 times that of non-planar chalcogenide glass microspheres [4]. We also show that such resonators can be used as ultra-sensitive probes of photosensitivity in chalcogenide glass, providing an unprecedentedly high accuracy measurement (on the order of 10^{-8} RIU) of photorefractive index change. Monte-Carlo simulations and a peak fitting algorithm are employed to quantitatively assess the performance matrices as a function of cavity Q-factor and reasonable agreement with experiments is confirmed. We show that such a high wavelength resolution projects high sensitivity for both refractometry-based biological sensing and evanescent wave-based chemical detection.

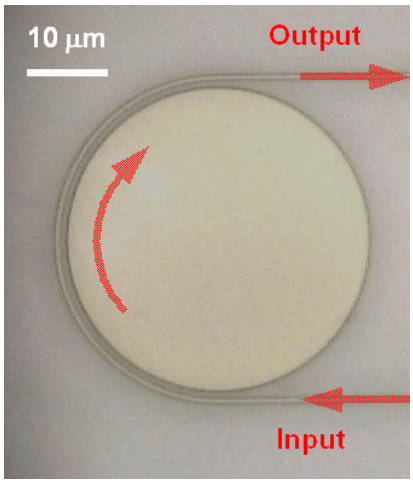

▲ Figure 1: Optical micrograph of a 20-µm-radius pulley-type As_2S_3 microdisk resonator.

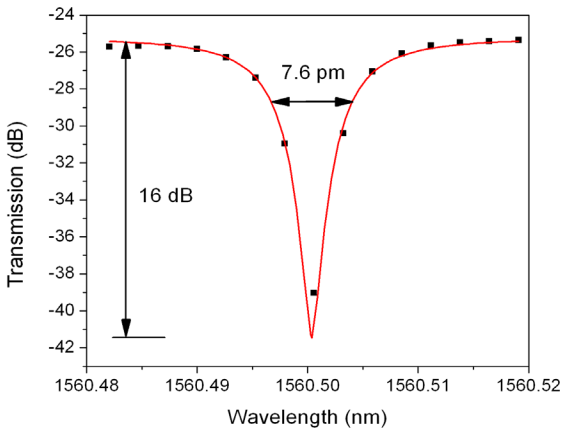

▲ Figure 2: A transmission spectrum near a TM-polarization resonant peak: the black dots are experimental data points and the red curve is the fitted Lorentzian peak.

References

[1] J. Hu, V. Tarasov, N. Carlie, N. Feng, L. Petit, A. Agarwal, K. Richardson, and L. Kimerling, "Si-CMOS-compatible lift-off fabrication of low-loss planar chalcogenide waveguides," *Optics Express*, vol. 15, p. 11798, 2007.

[2] Y. Ruan, M. Kim, Y. Lee, B. Luther-Davies, and A. Rode, "Fabrication of high-Q chalcogenide photonic crystal resonators by e-beam lithography," *Applied Physics Letters*, vol. 90, p. 071102, 2007.

[3] J. Hu, N. Carlie, L. Petit, A. Agarwal, K. Richardson, and L. Kimerling, "Demonstration of chalcogenide glass racetrack micro-resonators," *Optics Letters*, vol. 33, p. 761, 2008.

[4] G. Elliott, D. Hewak, G. Murugan, and J. Wilkinson, "Chalcogenide glass microspheres: Their production, characterization and potential," *Optics Express*, vol. 15, p. 17542, 2007.

Digital Equalization of the Nonlinear Photonic Modulator Diode

B. Moss, A. Joshi, J. Orcutt, V. Stojanović
Sponsorship: DARPA, Texas Instruments

Electro-optical modulators are fundamental building blocks in on-chip photonic systems. On-chip optical waveguides can be created from thin unsilicided polysilicon tracks in a bulk CMOS process. The index of refraction of the poly waveguide depends on the charge concentration in the waveguide. Varying this charge concentration changes the phase of the light through the waveguide. In order to inject large amounts of charge into the waveguide more effectively, a P-I-N diode structure is created with the waveguide acting as the intrinsic region (I region) and N- and P-type doping added on either side of the waveguide.

We modified an existing SPICE model [1-2] of a P-I-N diode to model the photonic modulator. Figure 1 shows a digital circuit that controls the amount of charge entering the I region. This circuit uses a push-pull topology with pre-emphasis. The pre-emphasis controls the amount of charge that must enter and leave the I region for each bit, lowers the energy per bit, and prevents the ring's optical passband from shifting into the next optical channel. At the beginning of a zero-to-one transition, both the strong driver and the weak driver are active, maximizing the current into the I region. After a short time, the strong driver deactivates, lowering the current into the diode. The unbalanced weak driver has a strong NMOS and a weak PMOS. The strong NMOS ensures that the device quickly discharges through the I region for a one-to-zero transition. Figure 2 shows the simulated eye diagram for 10Gb/s.

Two flavors of this ring modulator were taped out with a 65-nm TI process. One modulator has a larger weak driver to account for varying carrier lifetimes in the diode. The energy efficiency is predicted to be approximately 50 fJ/bit.

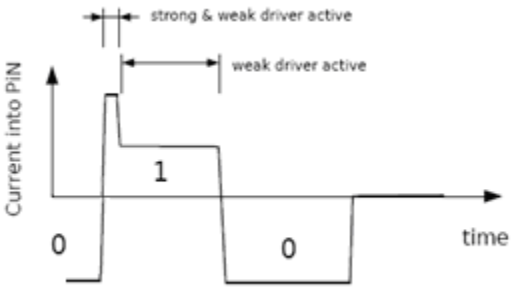

▲ Figure 1: Abstract modulator diagram and its corresponding pre-emphasized current profile for a 010- input bit pattern. The weak driver has a very strong NMOS and a weak PMOS.

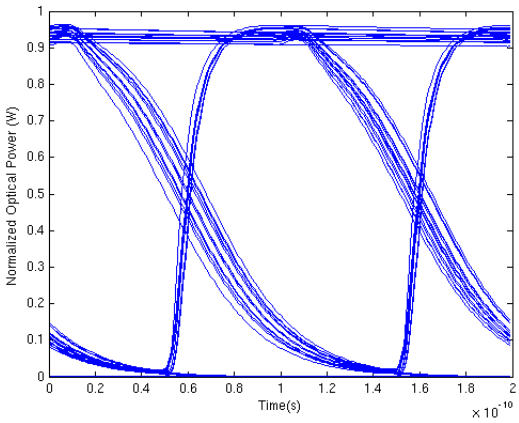

▲ Figure 2: Simulated eye diagram for 10Gb/s, assuming a 1-ns carrier lifetime.

References

[1] A.G.M. Strollo, "A new SPICE model of power P-I-N diode based on asymptotic waveform evaluation," *IEEE Transactions on Power Electronics*, vol. 12, no. 1, pp. 12-20, Jan. 1997.

[2] J. Kyhala and M. Andersson, "An advanced PIN-diode model," *Microwave Journal*, vol. 48, no. 9, pp. 206-212, Sept. 2005.

High-speed Large-area Ge Photodetectors on Si

J. Cheng, W. Giziewicz, J. Liu, C.-Y. Hong, L.C. Kimerling, J. Michel

We have designed and demonstrated lateral Ge p-i-n photodiodes on Si with 100-μm and 200-μm diameters and GHz bandwidth working at 850 nm. These lateral devices demonstrate a significant bandwidth improvement compared to vertical junction devices of the same area due to the reduction of capacitance. The devices were fabricated with 500-nm CMOS process technology, which enables large scale production at relatively low cost compared to III-V devices.

Figure 1 shows the structure of a lateral Ge-on-Si photodetector schematically. A lateral detector with interdigitated electrode is chosen over vertical junction detectors because of much lower capacitance per unit device area. The simulations done by MEDICI software show that a normalized external quantum efficiency of 71% can be achieved. The bandwidths are examined for 50-, 100- and 200-μm diameter devices with different finger spacings. Devices on n-type substrates have high bandwidth due to the full depletion of the inter-finger region. For a 100-μm-diameter device, a 10-Gb/s data rate can be reached at a relatively low voltage of 3V [1].

The devices were fabricated completely on a standard 0.5-μm CMOS line[2]. The frequency responses of the detectors are carried out by an Agilent N5230A Vector Network Analyzer using a 850-nm VCSEL. Figure 2 shows the frequency response of the photodetectors with different diameters and finger spacings. The 100-μm -diameter devices reach 6-GHz bandwidth, while devices with 200 μm diameters reach 2.2 GHz. These bandwidths are about 5 times higher than ideal vertical detectors with the same Ge film thickness and contact pad area.

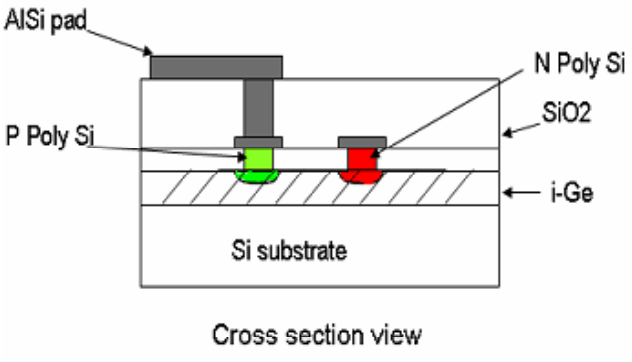

▲ Figure 1: Schematic structure of a lateral Ge p-i-n photodetector on Si.

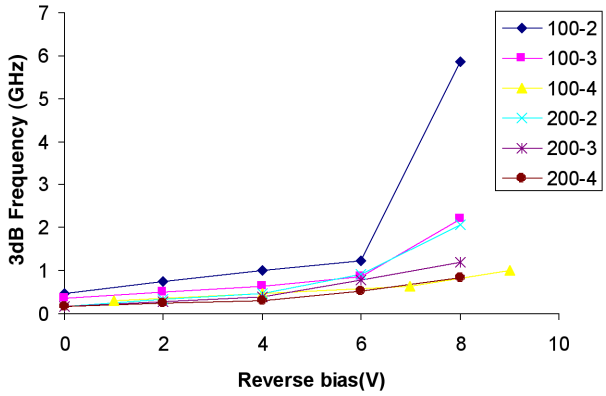

▲ Figure 2: Frequency response of lateral Ge p-i-n devices.

References

[1] W. Giziewicz, "High performance photodetectors for multimode optical data links," Ph.D. thesis, Massachusetts Institute of Technology, Cambridge, 2006.

[2] J.F. Liu, J. Michel, W. Giziewicz, D. Pan, K. Wada, D. Cannon, L.C. Kimerling, J. Chen, F.O. Ilday, F.X. Kartner, and J. Yasaitis, "High-performance, tensile-strained Ge p-i-n photodetectors on a Si platform," *Applied Physics Letters*, vol. 87, no. 10, pp. 103501:1-3, Sept. 2005.

Recess Integration of GaN LEDs on Si IC Micro-probes for Optical Control of Excitable Cells

H. Soumare, C.G. Fonstad (in coll. with E. Boyden, MIT)
Sponsorship: MIT Media Lab Director's Innovator Award

Professor Ed Boyden uses light to precisely control aberrant neuron activity. His lab has invented safe, effective ways to deliver light-gated membrane proteins to neurons and other excitable cells (e.g., muscle, immune cells, pancreatic cells, etc.) in an enduring fashion, thus making the cells permanently sensitive to being activated or silenced by millisecond-timescale pulses of blue and yellow light, respectively [1]. This ability to modulate neural activity with a temporal precision that approaches that of the neural code itself holds great promise for human health, and his lab has developed animal models of epilepsy and Parkinson's disease to explore the use of optical control to develop new therapies. His work has attracted international attention and has appeared in numerous articles, including a recent piece in the Science Times section of the New York Times [2], and a profile of his lab for the Discovery Channel's "Top 5 Science Stories of the Year."

The powerful micro-hybrid assembly and integration techniques that Professor Fonstad's group has recently developed and used to integrate vertical cavity surface emitting lasers (VCSELs) within silicon CMOS integrated circuits, and edge-emitting laser diodes with dielectric waveguides on silicon wafers, provide a path to making needle probes with many individually addressable blue and yellow micro-LEDs spaced along their length. An LED needle like this with ten to twenty micro-LED pairs would be similar in diameter to a single optical fiber like those now being used by Professor Boyden, yet it would serve the function of many fibers and, in fact, would enable researchers to conduct studies that are impossible to do with a single fiber, or even with multiple fibers. The same needle could also have electrodes along it to simultaneously monitor electrical activity in the stimulated regions, on-board CMOS electronics to control all functions, and cooling channels to eliminate all thermal impact.

Professors Boyden and Fonstad have initiated collaborative efforts to develop such a probe, with the immediate target being a simpler probe with LEDs and electrodes, with all external control and signal processing electronics. This probe will address all of the key challenges, so that future expansion to integrated electronics and cooling will be possible.

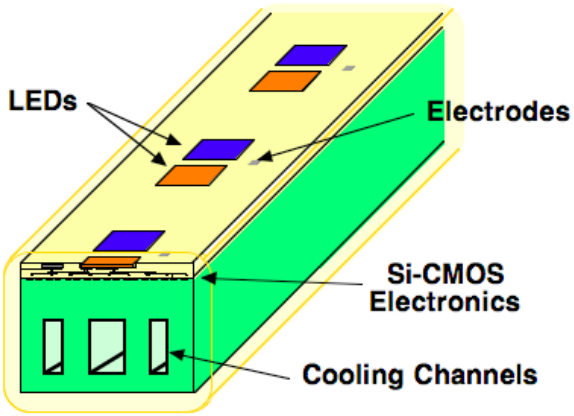

▲ Figure 1: A cartoon illustrating the LED needle probe that is the ultimate target of this research program. The initial needles will be passive without integrated electronics or cooling, and the focus of the program will be on developing micro-pill LEDs (see Figure 2) suitable for use with the recess integration technology that has been developed at MIT. The work will ultimately be extended to active IC foundations.

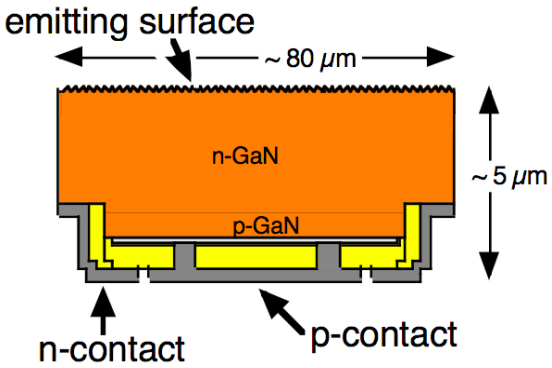

▲ Figure 2: A cross-sectional cartoon (not to scale) of an LED micro-pill. The pill thickness will be 5 to 6 microns and the width will be 80 to 100 microns. Both n-side and p-side contacts are made to same side of the pill and the upper emitting surface is roughened to enhance light extraction.

References

[1] X. Han and E.S. Boyden, "Multiple-color optical activation, silencing, and desynchronization of neural activity, with single-spike temporal resolution," PLoS ONE 2(3): e299. DOI: 10.1371/journal.pone.0000299.

[2] *The New York Times*, Science Section, Aug. 14, 2007, p. D1.

Co-axial Integration of III-V Ridge-waveguide Gain Elements with SiO_xN_y Waveguides on Silicon

J. Diaz, S. Famenini, E. Barkley, J. Rumpler, J. Perkins, C.G. Fonstad
Sponsorship: Vitesse Chair

Our ongoing research integrating 1.55-μm III-V ridge waveguide gain elements (i.e., diode lasers and semiconductor optical amplifiers) co-axially aligned with and coupled to silicon oxy-nitride waveguides on silicon substrates has made significant strides in the past year. We are working towards the goal of co-axially coupling III-V laser diodes and semiconductor optical amplifiers with waveguides on Si wafers using techniques consistent with fabricating waveguides on Si-CMOS wafers and integrating the III-V gain elements after all standard front- and back-end Si processing has been completed.

A novel micro-cleaving technique has been used to produce active ridge waveguide platelets on the order of 6 μm thick and 100 μm wide, with precisely controlled lengths (in the current work 300 ± 1.25 μm) and very high-quality end facets. Typical ridge guide platelet lasers have thresholds under 30 mA.

Passive micro-cleaved platelets have been integrated within dielectric recesses etched through the oxy-nitride (SiO_xN_y) waveguides on a wafer so the ridge and SiO_xN_y waveguides are co-axially aligned. Transmission measurements indicate coupling losses are as low as 5 db with air filling the gaps between the waveguide ends, and measurements made through filled gaps indicate that the coupling losses can be reduced to below 1.5 dB with a high index (n = 2.2) dielectric fill. Simulations indicate that with further optimization of the mode profile in the III-V waveguide the loss can be reduced to below 1 dB.

We have also performed extensive device design and optimization for co-axial recess integration and have recently completed a comparison of co-axial coupling with the evanescently coupled III-V/Si hybrid integration approach recently introduced by researchers at UCSB and Intel. The latter comparison revealed that the approach we have taken, co-axial end-fire coupling, and the UCSB/Intel approach, vertical evanescent coupling, are complementary, with each optimal for certain applications. At the same time it pointed out a number of distinct advantages for co-axial coupling of recess-integrated platelet lasers including higher operating efficiency, smaller device footprint, greater flexibility in choice of materials, lower cost, higher modularity, and easier integration of different wavelength emitters [1].

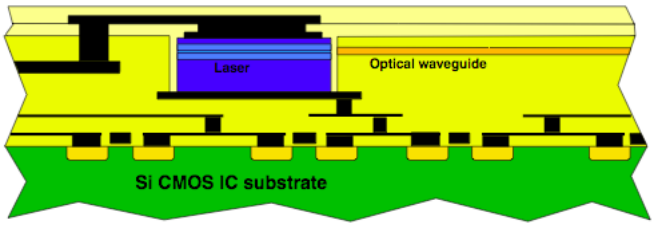

▲ Figure 1: A cartoon illustrating the recess-mounting and co-axial alignment approach to integrating III-V gain elements (edge-emitting in-plane laser diodes, EELs, and semiconductor optical amplifiers, SOAs) with silicon oxy-nitride waveguides on silicon integrated circuit chips and silicon photonic integrated circuits platforms.

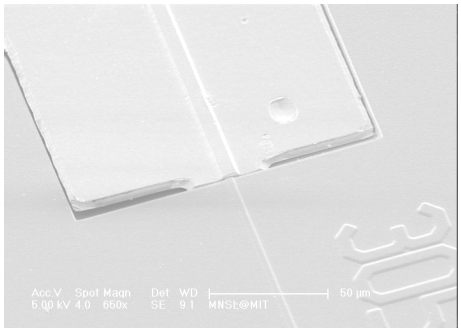

▲ Figure 2: A close-up photomicrograph showing the alignment between a InGaAsP/InP ridge waveguide platelet and a buried silicon oxy-nitride waveguide. Coupling losses as low as 3 dB were measured.

References

[1] C.G. Fonstad, J.J. Rumpler, E.R. Barkley, J.M. Perkins, and S. Famenini, "Recess integration of micro-cleaved laser diode platelets with dielectric wave-guides on silicon," in *Proc. Novel In-plane Semiconductor Lasers Conference VII, Photonics West 2008,* Jan. 22, 2008; *SPIE Conference Proc.*, vol. 6909.

Magnetically-assisted Assembly, Alignment, and Orientation of Micro-scale Components

D. Cheng, J. Perkins, J. Rumpler, C.G. Fonstad (in coll. with F. Cadieu, Queens College of CUNY; M. Zahn, MIT)
Sponsorship: Vitesse Chair

The use of magnetic forces to improve fluidic self-assembly of micro-components has been investigated using Maxwell 3D to model the forces between Ni thin films on semiconductor device micro-pills and Sm-Co thin films patterned on target substrates. Orienting and restraining forces on pills far in excess of gravity are predicted, and it is found that the fall-off of these forces with pill-to-substrate separation can be engineered through the proper design of the Sm-Co patterns to retain only properly oriented pills [1].

Micro-scale hybrid assembly is a potentially important way of doing heterogeneous integration, i.e., of integrating new materials on silicon integrated circuits to obtain functionality not readily available from silicon device structures alone, and fluidic self-assembly is an attractive way to automate micro-scale assembly. A serious limitation of fluidic self-assembly, however, is the lack of a good method for holding properly assembled components in place and accurately positioned until all of the components have been assembled and they have been permanently bonded in place. We have shown, based on our modeling, that suitably patterned magnetic films can be used to provide the forces necessary to retain, and to accurately orient and position, assembled micro-components.

Our motivation for pursuing micro-scale hybrid assembly is our general interest in doing optoelectronic integration, specifically of vertical cavity surface emitting lasers (VCSELS), edge-emitting lasers (EELs), and light emitting diodes (LEDs), with state-of-the-art, commercially processed Si-CMOS integrated circuits. Our ongoing research integrating these devices on silicon described elsewhere in this report provides the context for this work and illustrates the types of applications we envision for magnetically assisted self-assembly using the results of this study.

Assembly experiments to verify and demonstrate the theoretical predictions are currently in progress using two sizes of 6-μm thick pills (50 μm by 50 μm, and 50 μm by 100 μm), and a variety of magnetic thin film patterns. Recesses with different dimensions are also being studied.

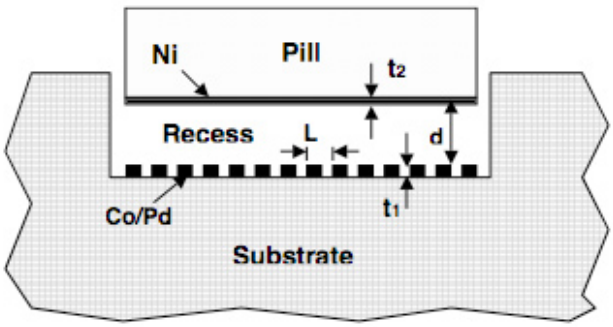

▲ Figure 1: A cross-sectional cartoon illustrating the application of magnetically assisted assembly to recess integration. The variables indicated in the drawing correspond to the model used to calculate the magnetic force intensity.

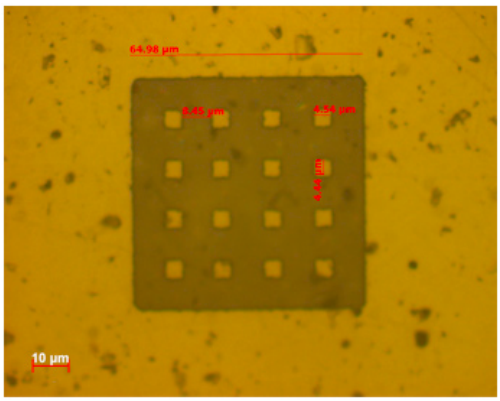

▲ Figure 2: A microphotograph of a patterned samarium cobalt magnetic thin film. The abilities to, first, sputter deposit, and second, wet etch thin films like this are critical to the successful implementation of magnetic self-assembly and are unique strengths of the MIT/Queens College effort.

References

[1] D. Cheng, C.G. Fonstad, and M. Zahn, "Simulation and design of forces during magnetically assisted fluidic self-assembly," *Ansoft First-Pass System Success Application Workshop*, Oct. 19, 2007, Newton, MA (invited talk and poster).

[2] D. Cheng, "Theoretical and experimental study of magnetically assisted fluidic self assembly," Master's thesis, Massachusetts Institute of Technology, Cambridge, 2008.

Micro-cleaved Laser Diode Platelets Integrated on Silicon

J. Rumpler, C.G. Fonstad

Sponsorship: DARPA through ARL; Lincoln Laboratory IPI Program

Thin (6-μm) InP-based multiple-quantum-well (MQW) ridge laser platelets emitting at a wavelength of 1550 nm have been manufactured and integrated by metal-to-metal bonding onto silicon substrates. These laser platelets can be thought of as freestanding optoelectronic building blocks that can be integrated as desired on diverse substrates. These blocks are fully processed lasers, with both top-side and bottom-side electrical contacts. The thinness of these optoelectronic building blocks and the precision with which their dimensions are defined are conducive to assembling them in dielectric recesses on a substrate, such as silicon, as part of an end-fire coupled optoelectronic integration strategy [1]. They are assembled by a micro-scale pick-and-place technique that allows the blocks to be picked up individually and placed as desired on the substrate of choice. Final integration is accomplished using pressurized polymer film to hold the platelets in place as they are metal-to-metal solder bonded to the Si substrate.

To enable the manufacture of these laser platelets, a novel micro-cleaving process technology has been developed that uses notched bars of lasers as shown in Figure 1 to accurately locate the point of cleavage. This novel micro-cleaving process is used to simultaneously obtain both smooth end facets and precisely defined cavity lengths. As a proof of concept, this process has been shown to achieve nominal cavity lengths of 300 μm +/- 1.25 μm. We believe that this micro-cleaving process can be used to make thin platelet lasers having much shorter cavity lengths and that with minor adjustments it can be used to achieve better than 1-μm length precision.

For the 300-μm-long, 6-μm-thin, micro-cleaved ridge platelet lasers integrated onto silicon substrates, as shown in Figure 2, continuous-wave lasing at temperatures as high as 55 °C and pulsed lasing at temperatures to at least 80 °C have been achieved. These lasers have output powers as high as 26.8 mW (at T = 10.3 °C), differential efficiencies as high as 81% (at T = 10.3 °C), and threshold currents as low as 18 mA (at T = 10.3 °C). The characteristic temperatures, T_0 and T_1, of the lasers on silicon were 43 K and 85 K, respectively. The thin micro-cleaved ridge platelet lasers integrated onto silicon outperformed conventionally cleaved multiple-quantum-well (MQW) ridge lasers on their native InP substrate in terms of thermal characteristics, output power, and differential efficiency [2].

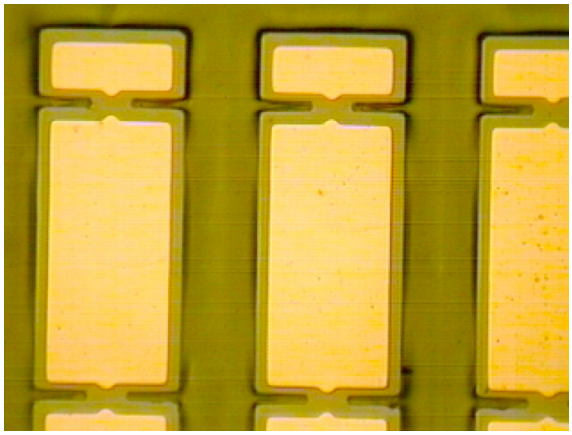

▲ Figure 1: A back-side view of platelet lasers bars after front-side processing has been completed and the wafer has been mounted face-down on a carrier wafer, the substrate removed, and the back-side metal deposited and patterned. The bars will next be released and micro-cleaved to produce individual platelet lasers approximately 150-μm wide and 300-μm long.

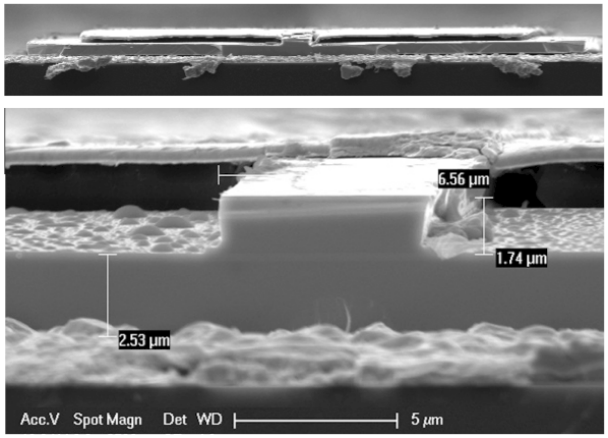

▲ Figure 2: Close-up photomicrographs showing, in the top portion of the figure, a platelet bonded on a silicon wafer. A close-up view of the micro-cleaved end facet and the ridge waveguide is shown in the lower portion of the figure. Note also the stripe ohmic contact on top of the mesa and the broad-area top contact pad (insulated by a BCB support layer).

References

[1] C.G. Fonstad, J.J. Rumpler, E.R. Barlkley, J.M. Perkins, and S. Famenini, "Recess integration of mirco-cleaved laser diode platelets with dielectric wave-guides on silicon," in *Proc.Novel In-plane Semiconductor Lasers Conference VII, Photonics West 2008*, Jan. 22, 2008; SPIE Conference Proc. vol. 6909.

[2] J.J. Rumpler II, "Micro-cleaved ridge lasers for optoelectronic integration on silicon," Ph.D. Thesis, Massachusetts Institute of Technology, Cambridge, 2008.

Low-threshold Vertical Cavity Surface-emitting Lasers Recess Integrated within Silicon CMOS Integrated Circuits

J.M. Perkins, C.G. Fonstad

Sponsorship: NSF

Optoelectronic devices intimately integrated on silicon integrated circuits have long been sought for optical intercon-nect applications in an effort to improve data transfer rates in high performance circuits. A new heterogeneous integration technique for integrating vertical cavity surface emitting lasers (VCSELs) on silicon CMOS integrated circuits for such applications has been developed and demonstrated for the first time in our group at MIT [1, 2].

Fully processed and tested oxide-aperture VCSELs emitting at 850 nm have been fabricated as individual "pills" 55 μm in diameter and 8 μm tall with a disk contact on the n-type backside and a ring contact on the p-type, emitting top-side. With a custom micro-pipette vacuum pick-up tool, these pills are placed on contact pads at the bottom of recesses etched though the dielectric over coating on a Si-CMOS chip, and when all the recesses on the chip are filled the pills are batch-solder-bonded in place. Back-end processing of the chip then continues with surface planarization, contact via formation, and interconnect metal deposition and patterning. A completely integrated pill appears in Figure 1.

The integrated VCSEL characteristics appear in Figure 2. They have threshold currents of 1 to 2.5 mA and thermal impedances as low as 1.6 °C per mW, both of which are similar to native substrate device thresholds and impedances. Thermal modeling of these devices has also been preformed, investigating the impact of integration on VCSEL device operation. The results show potential thermal impedance improvements for both single and arrayed devices due to integration on silicon. This model also investigates the impact of integration on a dielectric stack, as well as the impact of the current aperture of the VCSEL device.

The technique demonstrated in this work integrates devices as individual pills within the dielectric stack covering a Si IC, allowing for wafer-scale monolithic processing of heterogeneous circuits. The process effectively avoids thermal expansion mismatch limitations, and it is compatible with parallel assembly techniques, such as fluidic self-assembly.

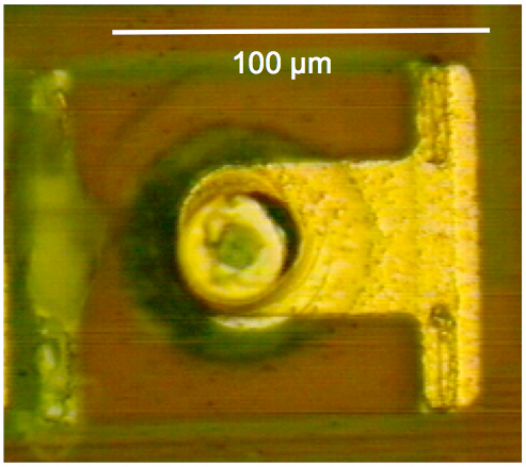

▲ Figure 1: A microphotograph of a fully integrated VCSEL in its recess on a CMOS chip showing the upper contact pattern connecting the VSCEL to the underlying circuitry. The emission comes from the small aperture in the contact pattern roughly in the center of the picture. Figure 2 shows the CW drive and output characteristics of the VCSEL.

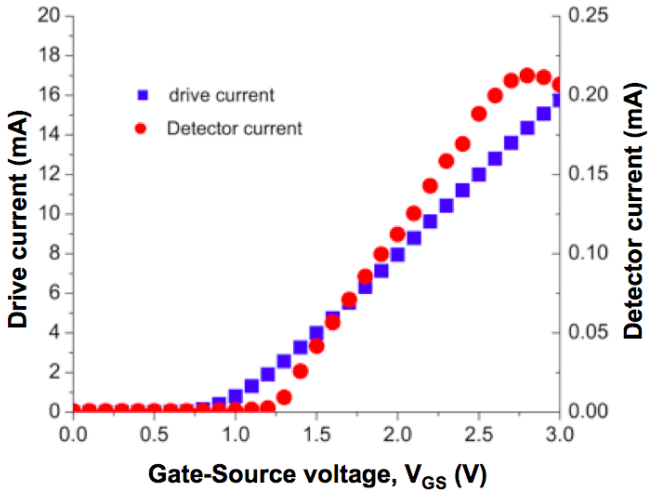

▲ Figure 2: The CW drive and output characteristics of an integrated VCSEL driven by an on-chip transistor circuit. The diode current (left axis) and optical output (detector current, right axis) are plotted as a function of the gate-to-source voltage applied to the n-MOS drive transistor. The MOSFET threshold voltage is ~ 1 V, and the VCSEL threshold is ~ 2 mA.

References

[1] J.M. Perkins and C.G. Fonstad, " Full recess integration of small diameter low threshold VCSELs within Si-CMOS ICs," in review.

[2] J.M. Perkins, "Low threshold vertical cavity surface emitting lasers integrated onto Si-CMOS ICs using a novel hybrid assembly technique," Ph.D. thesis, Massachusetts Institute of Technology, Cambridge, 2007.

Magnetic Oxides for Optical Isolators and Magnetoelectronic Devices

C.A. Ross, G.J. Dionne, A. Taussig, L. Bi, V. Sivakumar, H.S. Kim
Sponsorship: Lincoln Laboratory, ISN, NSF

We have established a thin-film laboratory that includes a pulsed-laser deposition (PLD) system and an ultra-high vacuum sputter/analysis system. In PLD, a high-energy excimer laser is used to ablate a target, releasing a plume of material that deposits on a substrate to form a thin film. The PLD is particularly useful for making complex materials such as oxides because it can preserve the stoichiometry of the target material.

We have been using PLD to deposit a variety of oxide films for magneto-optical devices such as isolators. These materials include iron oxide, which can adopt one of four different ferrimagnetic or antiferromagnetic structures depending on deposition conditions, and bismuth iron garnet (BIG, $Bi_3Fe_5O_{12}$), which is useful for magneto-optical isolators in conventional photonic devices. The ideal material for an isolator combines high Faraday rotation with high optical transparency. Garnets have excellent properties but do not grow well on silicon substrates, making it difficult to integrate these materials. In contrast, iron oxide (maghemite), with its high Faraday rotation, grows very well on MgO or Si, but its optical absorption is high. One way to solve this problem is to develop new magneto-optical active materials, which can grow epitaxially on Si by using buffer layers. When doped with transitional metal ions, these materials can exhibit strong Faraday rotation as well as low optical loss. Recently, we have examined Co-doped CeO_2 thin film (Figure 1) [1], which shows strong magneto-optical properties and lower optical absorption compared with iron oxide. The best figure of merit of 0.25 deg/dB, which is defined as Faraday rotation divided by optical absorption loss at 1550-nm wavelength, has been achieved in $Ce_{0.98}Co_{0.02}O_2$. Another investigation was carried out on Co- or Fe-doped SnO_2. As a material used for transparent conductive electrodes, SnO_2 can grow epitaxially on sapphire substrates. When doped with Co or Fe, this material shows Faraday rotation and low optical loss at 1550-nm wavelength. A figure of merit of 0.16 deg/dB is achieved in $Sn_{0.9}Co_{0.1}O_2$ (Figure 2). These films could be useful for waveguide isolators and other magnetoelectronic devices in which optical absorption losses are critical. A second project involves the use of electrochemical methods to control the magnetization of iron oxide spinel structure films (magnetite or maghemite) grown on conducting substrates, making a chemically-switchable material. The insertion of Li ions by electrochemical discharge changes the oxidation state of the Fe(III) to Fe(II) and can reduce the magnetization of the film by about 30%, in a reversible process. Recent experiments on nanoparticles of iron oxide show much greater changes in magnetization, up to ~80%, indicating that the process is kinetically limited. Lithiation of CrO_2 also successfully changes the magnetization, with an initial change of $5\mu_B$ per Li^+ ion insertion.

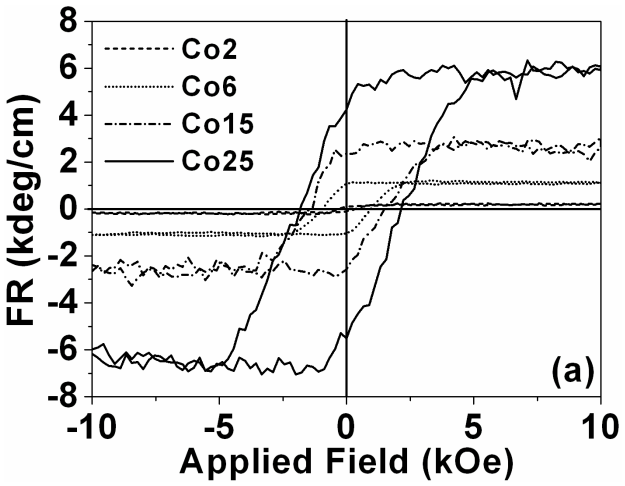

▲ Figure 1: Faraday rotation at 1550-nm wavelength vs. applied field for cobalt doped CeO_2 films grown on MgO (001) substrates. The Co2, Co6, Co15 and Co25 stand for 2 at%, 6 at%, 15 at%, and 25 at% of Co doping on the Ce sites, respectively.

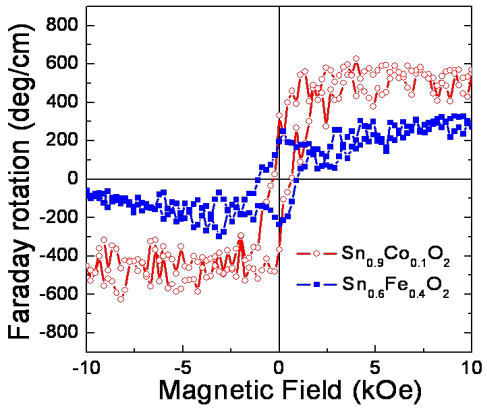

▲ Figure 2: Faraday rotation of $Sn_{0.9}Co_{0.1}O_2$ and $Sn_{0.6}Fe_{0.4}O_2$ films grown on R-plane sapphire substrates.

Reference

[1] L. Bi, H.-S. Kim, G.F. Dionne, S.A. Speakman, D. Bono, and C.A. Ross, "Structural, magnetic and magneto-optical properties of Co doped $CeO_{2-\delta}$ films," *Journal of Applied Physics*, vol. 103, no. 7, pp. 07D138:1-3, Mar. 2008.

Development of Terahertz Quantum Cascade Lasers

B. Williams, S. Kumar, A. Lee, Q. Qin, W. Kao, Q. Hu (in coll. with J. Reno, Sandia National Laboratories)
Sponsorship: NSF, NASA, AFOSR

The terahertz frequency range (1-10 THz) has long remained undeveloped, mainly due to the lack of compact, coherent radiation sources. Transitions between sub-bands in semiconductor quantum wells were suggested as a method to generate long wavelength radiation at customizable frequencies. However, because of difficulties in achieving population inversion between narrowly separated sub-bands and mode confinement at long wavelengths, THz lasers based on intersub-band transitions were developed only very recently. We have developed THz quantum-cascade lasers based on resonant-phonon-assisted depopulation and using metal-metal waveguides for mode confinement. The schematics of both features are illustrated in Figure 1a. Based on the combination of these two unique features, we have developed many THz QCLs with record performance, including a maximum pulsed operating temperature at ~170 K (top-right), a maximum power of ~250 mW (bottom-right), and the longest wavelength (~190 μm) QCL to date without the assistance of magnetic fields (bottom-left).

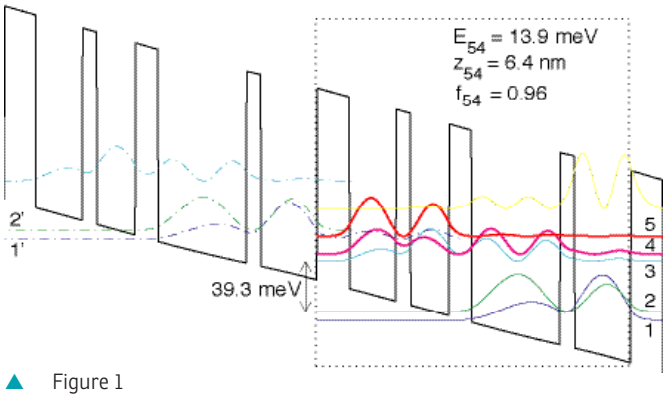

▲ Figure 1

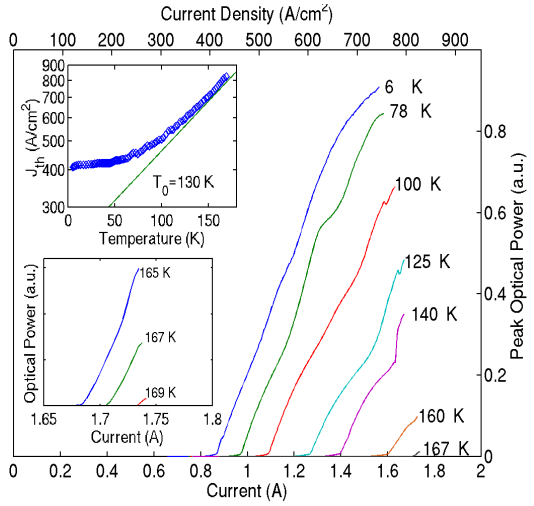

▲ Figure 2

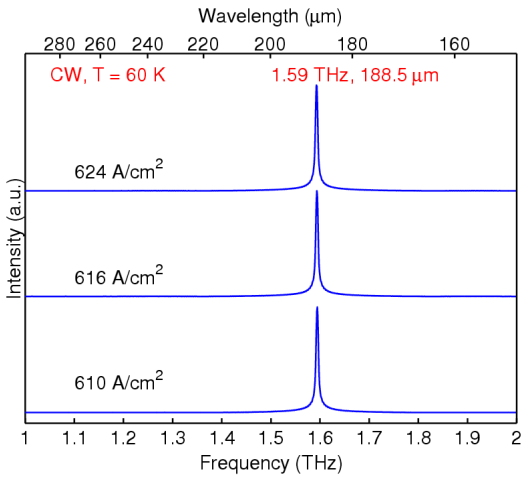

▲ Figure 3

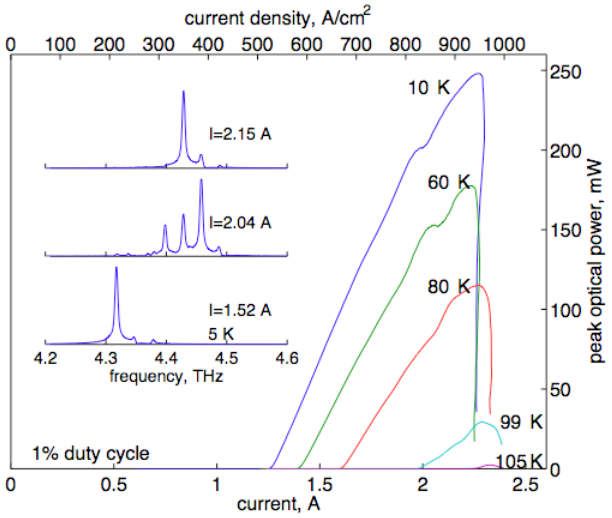

▲ Figure 4

Band-engineered Ge as a Gain Medium for Si-based Laser

X. Sun, J. Liu, L.C. Kimerling, J. Michel
Sponsorship: DARPA

Electronic-photonic Integrated Circuits (EPIC) based on Si microphotonics give a potential solution to solve the "interconnect" bottleneck problem that prevents Si microelectronics from further upgrading its performance by shrinking the dimensions [1]. An Si-based light emitter is one of the most important and challenging components for this EPIC architecture. We proposed and have studied Ge as active gain medium for a Si-based laser. H. Kroemer first discussed the possibility of achieving lasing in indirect band gap materials like germanium [2]. Our recent theoretical analysis has indicated that Ge can be band-engineered to behave like a direct bandgap material by introducing tensile strain and heavy n-type doping [3]. Figure 1 shows this process : 1) applying tensile strain in Ge to decrease the difference between the direct gap and the indirect gap and 2) n-type doping to fill the indirect L valley to make the two gaps electronically equal. Tensile strain gives an additional benefit of separating the light-hole valence band and the heavy-hole valence band at the band edge, as Figure 1 shows. This split facilitates the population inversion due to the lower density of states of the light-hole band, which can be more easily filled with injected holes. Practically, tensile strain can be introduced by the large thermal mismatch between Ge and Si up-cooling from the growth temperature to room temperature [4] and an n-type donor can be incorporated either during the Ge growth or by ion implantation. Detailed calculations have shown that this band-engineered Ge can provide optical gain at carrier injection levels comparable to III-V materials [3]. For example, the modeling shows that with a combination of 0.25% tensile strain and an extrinsic electron density of 7.6×10^{19} /cm^3 from n-type doping, a net material gain of ~400 cm^{-1} can be obtained from the direct bandgap transition of Ge despite the free carrier absorption loss. Photoluminescence (PL) measurement has been performed on band-engineered Ge thin films epitaxially grown on Si. Direct bandgap PL at around 1550 nm has been observed and the intensity is over 50 times larger than that of intrinsic Ge films on Si. The increase of the PL intensity with n-type doping confirms our theoretical predictions. The results indicate that such band-engineered Ge is a good candidate for a monolithically integrated Si-based laser.

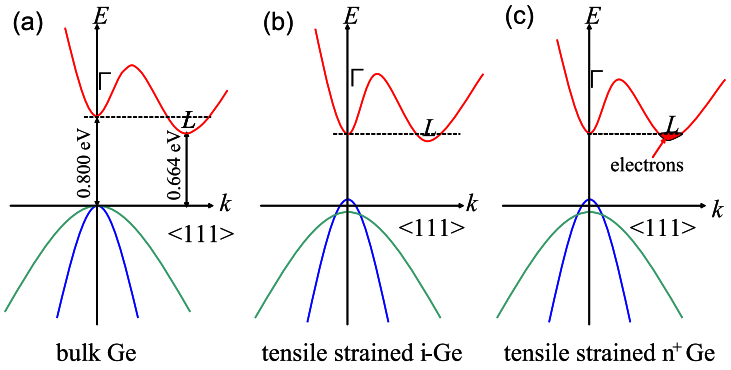

▲ Figure 1: Schematic band structure of bulk Ge shows a 136-meV difference between the direct gap and the indirect gap. This difference can be decreased by introducing tensile strain (0.25%), and the rest can be further compensated by filling electrons from n-type dopants (7.6×10^{19}/cm^3) into the L valley so that finally makes the two gaps electrically equal. [1]

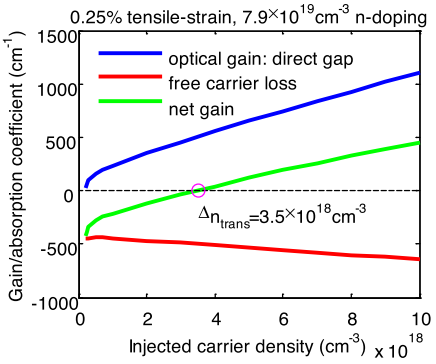

▲ Figure 2: Gain coefficient at 1560 nm was calculated for the same material at different excess carrier injection levels. Free carrier absorption, which dominates the material loss, was also calculated. The difference between gain and loss shows that the positive net gain is achieved above the transparency carrier density of 3.5×10^{18}/cm3, which is highlighted [1].

References

[1] L. Pavesi and D.J. Lockwood, *Si Photonics*. New York, NY: Springer, 2003.
[2] H. Kroemer, "A proposed class of heterojunction injection lasers," *Proc. of the IEEE*, vol. 51, no. 12, Dec. 1963, pp. 1782-1783.
[3] J. Liu, X. Sun, D. Pan, X.Wang, L.C. Kimerling, T L. Koch, and J. Michel, "Tensile-strained, n-type Ge as a gain medium for monolithic laser integration on Si," *Optical Express*, vol. 15, no. 18, pp. 11272-11277, Sept. 2007.
[4] D.D. Cannon, J. Liu, Y. Ishikawa, K. Wada, D.T. Danielson, S. Jongthammanurak, J. Michel, and L.C. Kimerling, "Tensile strained epitaxial Ge films on Si(100) substrates with potential application in L-band telecommunications," *Applied Physics Letters*, vol. 84, no. 6, pp. 906-908, 2004.

Electrical and Optical Characteristics of Selectively Grown Ge-on-Si Photodiodes

N. DiLello, J. Yoon, J.S. Orcutt, M. Kim, J.L. Hoyt
Sponsorship: DARPA, SRC student fellowship

Germanium is a promising candidate for use in CMOS-compatible photodiodes. Its strong absorption in the 1.55-μm range and relative ease of integration on silicon substrates make it suitable for telecommunications systems as well as in other high-speed electronic photonic integrated circuits. Important figures of merit in these photodiodes are the reverse leakage current and the responsivity. To reduce power consumption and improve the signal-to-noise ratio, it is important that the diodes have a low leakage current in reverse bias and a high responsivity, both typically quoted at -1 V. This study has investigated the leakage current of germanium photodiodes selectively grown by low-pressure chemical vapor deposition (LPCVD) using an Applied Materials epitaxial reactor.

To fabricate these diodes, 1 μm of germanium was grown by selective epitaxy on oxide-patterned *p+* Si wafers. Some wafers received an in-situ cyclic anneal to reduce the dislocation density, while others were unannealed. The wafers were then implanted with phosphorus to create a vertical *pin* junction and contacted with metal. Figure 1 shows a schematic diagram of the device cross-section (inset) and measured current vs. voltage characteristics for both the annealed and the unannealed wafers. The cyclic anneal reduces the leakage current at -1 V by a factor of approximately 5, on the lowest leakage diodes; however, the cyclic anneal also results in a larger distribution of the dark current. Figure 2 shows the photoresponse for various sizes of diodes from the annealed wafer with an applied bias of -1 V. The absorption edge shifts to longer wavelengths for larger devices, suggesting a smaller bandgap (shrinkage of ~25 meV) in the larger Ge areas, resulting from the induced strain in the film [1]. This behavior in the responsivity is consistent with Raman analysis, which shows higher strain in the larger-area devices.

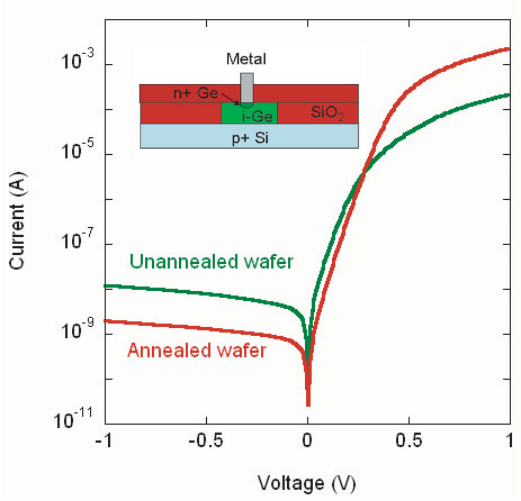

▲ Figure 1: Current vs. voltage characteristics for 5 x 10 μm rectangular diodes. The cyclic anneal reduces the leakage current by ~5x for the best performing diodes. There is a large variation in dark current for devices on the annealed wafer. The inset shows a cross-sectional schematic of the device.

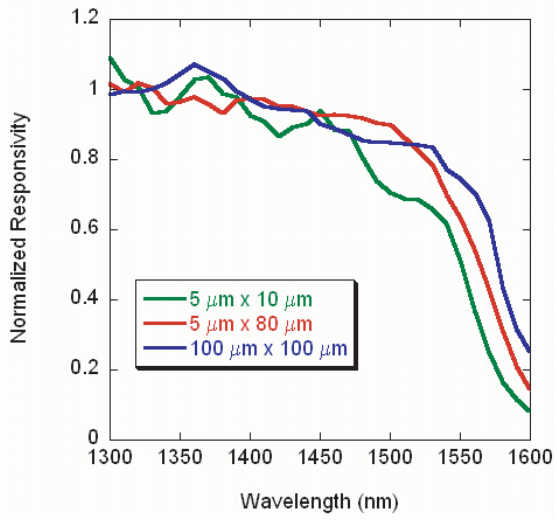

▲ Figure 2: Normalized responsivity vs. wavelength for various sizes of rectangular diodes. The photoresponse was normalized to an average of values taken in the 1300–1350-nm range. The absorption edge shifts to longer wavelengths for larger devices, corresponding to a smaller bandgap. This smaller bandgap is consistent with larger strain in the larger area devices.

Reference

[1] Y. Ishikawa, K. Wada, D.D. Cannon, J. Liu, H-C. Luan, and L.C. Kimerling, "Strain-induced band gap shrinkage in Ge grown on Si substrate," *Applied Physics Letters*, vol. 82, no. 13, pp. 2044-2046, Mar. 2003.

Excitonic Surface Plasmon Resonance Biosensor

M. Bora, K. Celebi, M.A. Baldo
Sponsorship: ISN

The main disadvantages of surface plasmon resonance (SPR) biosensors are their high cost and lack of portability. We propose to solve these deficiencies by integrating a plasmon source and detector with microfluidic components for a compact, inexpensive instrument. Surface plasmons are electromagnetic waves that propagate along a metal dielectric interface. The SPR biosensors exploit the sensitivity of surface plasmons to changes in the dielectric constant immediately adjacent to a metal surface. The angular reflectivity of the metal film has a sharp plasmon resonance feature that shifts when higher dielectric constant biomolecules bind to the surface. The high sensitivity of the SPR is complemented by real-time, label-free detection that provides additional information on the chemical kinetics of the interaction.

Here, we propose a novel surface plasmon biosensor that uses a plasmonic mode bound to the anode and cathode of a thin-film organic photovoltaic (PV). The sensor design combines the sensitivity of SPR with a novel plasmon conversion mechanism in the thin-film organic PV. The plasmon resonance is detected directly in the near field by coupling the electric field of the plasmon modes with exciton formation within the adjacent PV cell. The splitting of excitons into holes and electrons at the organic heterojunction interface of the PV cell generates a short circuit photocurrent modulated by the plasmon resonance condition set by the electric properties of the thin-film structure and the adjacent medium. Measurements of reflected power and photocurrent have a strong dependence on incident light angle, similar to the typical plasmon resonance curve. Agreement between this data and numerical simulations proves the existence of plasmon modes bound to the metal layers. The photocurrent generated by plasmon absorption in the photovoltaic is considerably larger than the optical absorption background. For sensing purposes, the photocurrent measured in our devices and reflectivity measured in standard SPR instrumentation are interchangeable and yield comparable sensitivity upon binding of biological species on the surface. We expect that this approach may replace large benchtop SPR sensors by sub-1-mm² devices compatible with array-processing of biological samples.

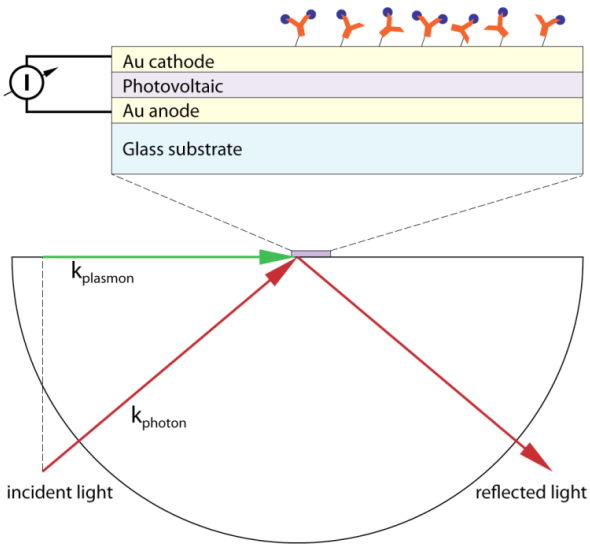

▲ Figure 1: Device structure and experimental setup. The P-polarized light falls on the photovoltaic structure at an angle controlled by the rotation of a hemi-cylindrical prism. Reflected power and current generated between the gold anode and cathode are monitored with respect to either incident angle or time for binding events on the top gold surface.

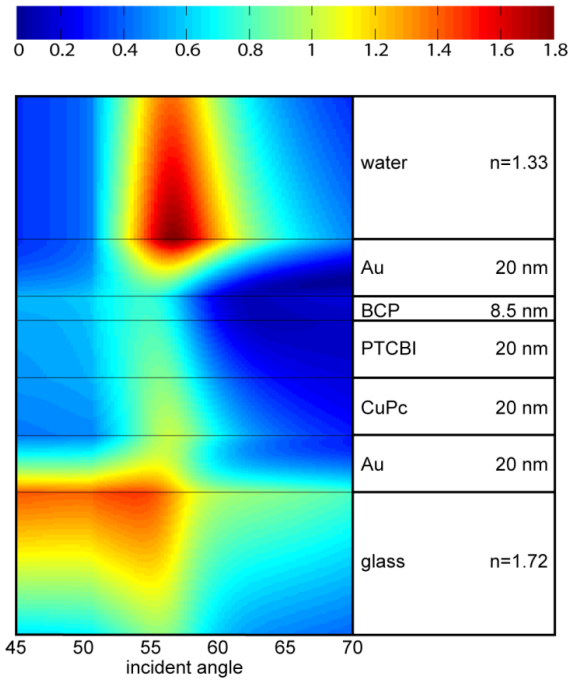

▲ Figure 2: Relative amplitude of the electric field for the transverse magnetic mode. Numerical simulations highlight the existence of a bound mode spanning the whole device structure. Plasmon excitations have the highest amplitude on the top surface of the cathode layer and extend in the organic layers of the photovoltaic.

Reference

[1] J.K. Mapel, K. Celebi, M. Singh, and M.A. Baldo, "Plasmonic excitation of organic double heterostructure solar cells," *Applied Physics Letters*, vol. 90, no. 12, pp. 121102:1-3, Mar. 2007.

Exciton-polaritons at Room Temperature in Metal-dielectric Microcavities

J.R. Tischler, M.S. Bradley, Y. Shirasaki, V. Bulović

Sponsorship: DARPA, NDSEG, MIT NSF MRSEC

Exciton-polariton-based photonic devices are a novel platform for realizing low-threshold lasing [1] and optical switching [2] in a scalable integrated architecture. Use of organic materials such as the excitonic component facilitates room-temperature operation of such devices [3]. Here we report room-temperature exciton-polariton devices consisting of layer-by-layer (LBL) assembled thin films of polyelectrolyte and the J-aggregates of the cyanine dye TDBC inserted in a resonantly-tuned planar $\lambda/2n$ optical microcavity with metal mirror and dielectric Bragg reflector (DBR). The device exhibits Rabi-splitting of $\Omega_R = 125 \pm 7$ meV with a polyelectrolyte/J-aggregate layer that is only 5.1 ± 0.5 nm thick [4]. Furthermore, the linewidth of the lower energy polariton state, measured on resonance, is $\Gamma = 12.1$ meV. The ratio $\Omega_R/2\Gamma = 5.1$ indicates that the device operates in a limit where the light-matter coupling (Ω_R) significantly exceeds competing dephasing processes (Γ). These figures of merit are achieved by virtue of the nanostructured film's large absorption coefficient of $\alpha \sim 1.0 \times 10^6$ cm^{-1} and by location of the 5.1 ± 0.5-nm-thick layer at the microcavity anti-node. Rabi-splitting and polaritonic dispersion are observed in the reflectance, transmittance, and photoluminescence measurements of the device. Because strong coupling is achieved with such thin films, the majority of the microcavity modal volume is available for integrating a variety of optically active materials, such as colloidal quantum dots and fluorescent polymers, into devices that could leverage the coherent properties of the strongly coupled states. Moreover, the LBL process provides nanometer-scale thickness control of ~1.7 nm per polymer/dye bilayer, suggesting that this device can be used to investigate fundamental physical phenomena such as non-radiative energy transfer and laser action in the strong coupling limit.

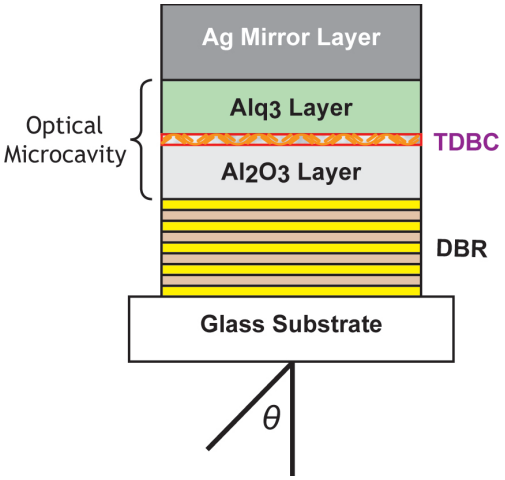

▲ Figure 1: Device design of polaritonic structure. Microcavity consists of a DBR and a silver mirror layer. On top of the J-aggregate layer, a film of small molecule Alq3 is thermally evaporated.

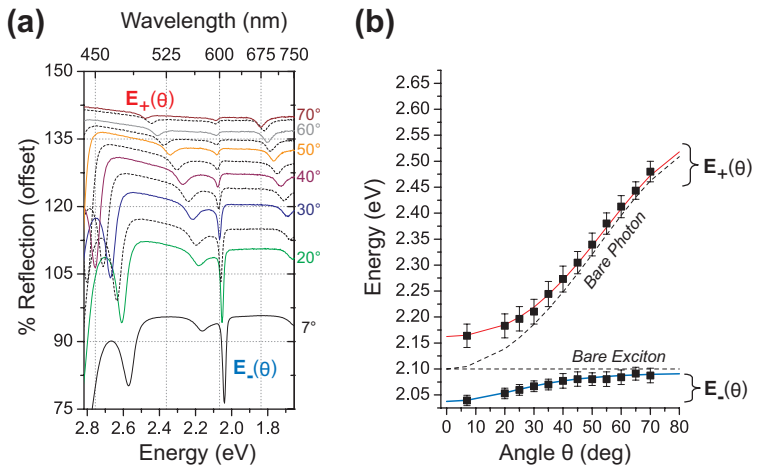

▲ Figure 2: (a) Angularly resolved reflectance measurements and (b) dispersion relation for resonantly tuned polaritonic structure. The microcavity is resonantly tuned at normal (at $\theta = 0°$) to the exciton resonance of 2.10 eV. The $E_-(\theta)$ denotes the lower energy polariton states; $E_+(\theta)$, the higher energy polariton states. Reflectance is measured with TE polarized incident light. Measurements from $\theta = 20°$ to 70° are relative values. Data at $\theta = 7°$ is absolute reflectance.

References

[1] S. Christopoulos, G.B. von Hogersthal, A.J. Grundy, P. Lagoudakis, A.V. Kavokin, J.J. Baumberg, G. Christmann, R. Butte, E. Feltin, J.F. Carlin, and N. Grandjean, "Room-temperature polariton lasing in semiconductor microcavities," *Physical Review Letters*, vol. 98, pp. 126405:1-4, Mar. 2007.

[2] N.A. Gippius, I.A. Shelykh, D.D. Solnyshkov, S.S. Gavrilov, Y.G. Rubo, A.V. Kavokin, S.G. Tikhodeev, and G. Malpuech, "Polarization multistability of cavity polaritons," *Physical Review Letters*, vol. 98, pp. 236401:1-4, June 2007.

[3] D.G. Lidzey, D.D.C. Bradley, M.S. Skolnick, T. Virgili, S. Walker, and D.M. Whittaker, "Strong exciton-photon coupling in an organic semiconductor microcavity," *Nature*, vol. 395, no. 6697, pp. 53-55, Sept. 1998.

[4] M.S. Bradley, J.R. Tischler, and V. Bulović, "Layer-by-layer J-aggregate thin films with a peak absorption constant of 10^6 cm^{-1}," *Advanced Materials*, vol. 17, no. 15, pp. 1881-1886, Aug. 2005.

Near-infrared J-aggregates for Exciton-polariton Optoelectronics

M.S. Bradley, J.R. Tischler, Y. Shirasaki, V. Bulović
Sponsorship: ISN, NDSEG, MIT NSF MRSEC

Thin films of J-aggregates of cyanine dyes, which found wide use in the 20th century in the photographic film industry, exhibit narrow linewidth and large oscillator strength, enabling their use in the first room-temperature solid-state electroluminescent devices that exhibit the strong-coupling regime of Cavity Quantum Electrodynamics (Cavity QED) [1]. As we demonstrated in a recent study, layer-by-layer (LBL)-assembled J-aggregate thin films can be precisely deposited in a specific location in a microcavity and contain a high density of aggregates, contributing to the observation of a peak thin-film absorption coefficient of 1.05 ± 0.1 x 10^6 cm^{-1}, among the highest ever measured for a neat thin film [2]. A recent study utilizing J-aggregates with exciton resonance in the near-infrared (NIR) spectral region demonstrated devices exhibiting strong coupling [3]. However, the J-aggregate films used were deposited by spin-coating, which results in nhomogeneous, thick films. In this work, we utilize the LBL deposition method to deposit thin films of these NIR J-aggregates, showing the same nanoscale thickness control and large peak thin-film absorption constant as observed in our previous studies for J-aggregates in the visible spectral region.

For deposition of thin films of NIR J-aggregates, substrates undergo sequential immersions in cationic and anionic solutions (SICAS). The cationic solution contains the very-low-molecular-weight polyelectrolyte PDAC (poly(dimethyldiallylammonium chloride)), and the anionic solution consists of the J-aggregating dye U3 (3-[(2Z)-5-chloro-2-[((3E)-3-{[5-chloro-3-(3-triethylammonium-sulfonatopropyl)-1, 3-benzothiazol-3-ium-2-yl]methylene}-2,5,5-trimethylcyclohex-1-en-1-yl) methylene]-1,3-benzqothiazol- 3(2H)-yl] propane-1-sulfonate). Figure 1 shows the reflectivity for films on glass substrates that underwent various numbers of SICAS, showing the NIR J-aggregate peak around λ=790 nm, as observed in [3] for spin-coated films. Figure 2 shows an atomic force microscopy (AFM) image of the 6.5 SICAS film, which demonstrates the remarkably-low (XYZ nm) roughness of films produced using this technique, which will allow for incorporation of these films into optical microcavities without contributing to significant inhomogeneous broadening of the cavity resonance, as needed for development of strongly-coupled Cavity QED devices.

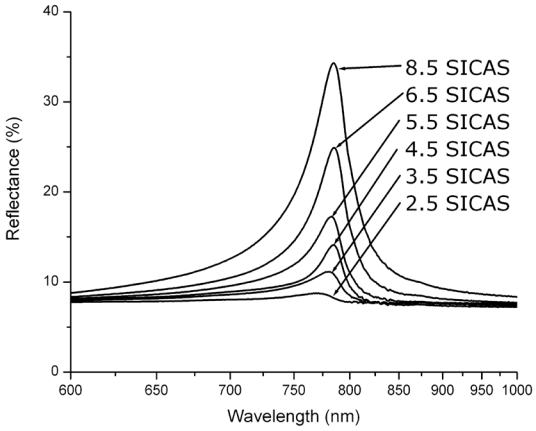

▲ Figure 1: Reflectance of thin films of NIR J-aggregates deposited on glass substrates using the LBL deposition method.

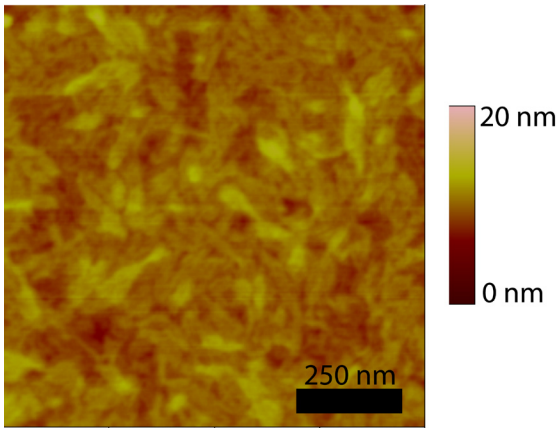

▲ Figure 2: AFM image of the 6.5 SICAS film from Figure 1. The low roughness allows incorporation of these films into microcavities without significantly increasing the nhomogeneous linewidth of the cavity resonance.

References

[1] J.R. Tischler, M.S. Bradley, V. Bulović, J.H. Song, and A. Nurmikko, "Strong coupling in a microcavity LED," *Physics Review Letters*, vol. 95, no. 3, pp. 036401-036404, 2005.

[2] M.S. Bradley, J.R. Tischler, and V. Bulović, "Layer-by-layer J-aggregate thin films with a peak absorption constant of 10^6 cm^{-1}," *Advanced Materials*, vol. 17, no. 15, pp. 1881-1886, 2005.

[3] J. Wenus, S. Ceccarelli, D.G. Lidzey, A.I. Tolmachev, J.L. Slominskii, and J.L. Bricks, "Optical strong coupling in microcavities containing J-aggregates absorbing in near-infrared spectral range," *Organic Electronics*, vol. 8, pp. 120-126, 2007.

Materials for Electro-optic Modulation and Switching

J. Hiltunen, D. Seneviratne, H.L. Tuller (in coll. with J. Yasaitis)
Sponsorship: Analog Devices, MIT Microphotonics Center

The drive towards integrated photonics requires the integration of various optical devices on a chip, including an optical modulator. Currently optical modulation with active waveguiding structures is implemented using $LiNbO_3$ single crystals. These devices require complex and expensive fabrication processes. In addition, their relatively low electro-optic coefficient leads to large component sizes, limiting miniaturization. The current demands for an increased degree of integration with cost-efficient device fabrication can be achieved using thin films of barium titanate.

The focus is on optimizing the electro-optic response of $BaTiO_3$ and related thin-film materials deposited by pulsed laser deposition (PLD) and sputtering onto single-crystal substrates directly or with buffer layers. A waveguide Mach-Zehnder interferometer structure, using a SiN strip-loaded waveguide, was prepared. We have demonstrated an effective electro-optic coefficient of 85pm/V, considerably greater than those available with bulk $LiNbO_3$ crystals. More recently $BaTiO_3$ (BTO) – $SrTiO_3$ (STO) multilayer thin-films of ~370-nm total thickness and varying stacking periodicity between 27 and 1670 Å were grown on single crystal MgO (001) substrates by PLD. The X-ray diffraction measurements confirmed the formation of BTO-STO super-lattices with a highly strained out-of-plane lattice parameter in the BTO layers due to interface-induced stress. Lattice strain relaxed with increasing layer thickness, resulting in reduced optical birefringence. The electro-optic response reached a maximum in films with stacking periodicity of 105 Å.

Micro-patterning Organic Thin Films via Contact Stamp Lift-off for Organic Light-emitting Device Arrays

J. Yu, V. Bulović

Sponsor: CMSE, PECASE

Patterning of organics in electronic devices is done primarily by techniques that are limited in resolution or scalability or are potentially damaging to the organic material. We demonstrate a simple subtractive stamping technique for patterning micron-sized features on organic thin films of nanometer-range thickness. Patterning is achieved by placing a relief-patterned polydimethylsiloxane (PDMS) stamp in contact with an organic film and peeling off the stamp (Figure 1a). The procedure is done without applied pressure or heat and can be done in an ambient environment, although a nitrogen environment is preferred for organic light-emitting device (OLED) fabrication. This technique is applied to pattern 13 micron-sized features of a two-color OLED structure.

To fabricate a two-colored OLED, a hole-blocking or emissive layer is patterned using this technique. The in-plane roughness of the patterned feature is shown in the height image of a patterned stripe (Figure 1b) and a profile of the patterned feature is shown (Figure 1c). Electroluminescence (EL) from blue-green device with 13-micron-sized features is shown (Figure 2a), and EL from blue-red devices of 25-micron-sized features is shown (Figure 2b). This technique can be applied twice to pattern blue-red devices with finer features (Figure 2c, d).

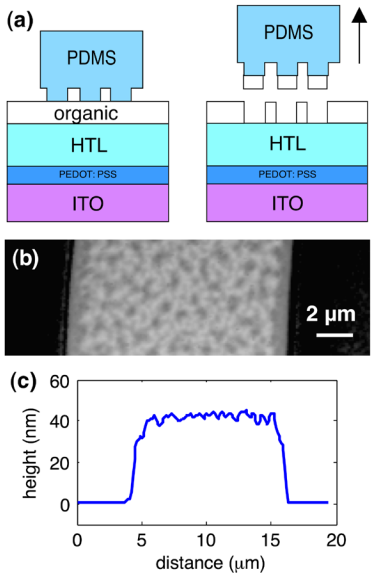

▲ Figure 1: (a) Demonstration of the subtractive stamping technique. Placing PDMS stamp to the substrate and subsequent release lifts off organic thin film from substrate surface. (b) Top view of in-plane patterned 20-nm TAZ on 50-nm TPD / PEDOT:PSS / ITO / glass substrate from AFM. (c) AFM height data to view lift-off patterned region.

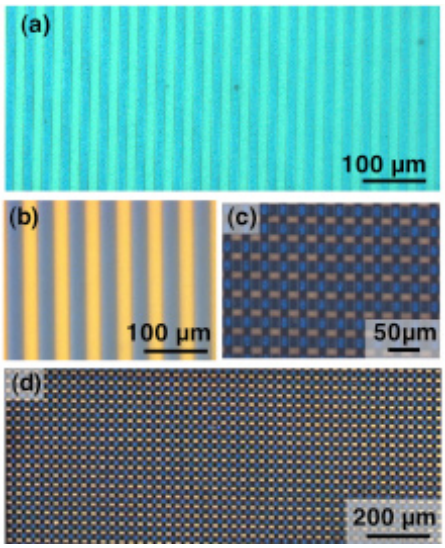

▲ Figure 2: (a) EL of green-blue OLED from patterned hole-blocking layer for AlQ_3 (green) or TPD (blue) emission. (b) EL of red-blue OLED from a patterned emissive layer DCM_2:AlQ_3 (red) or TPD (blue) emission and EL from red-blue patterned OLED by stamping twice to define finer features in (c) with a zoomed-out version (d).

Modeling of Electronic and Excitonic Processes in Quantum Dot LEDs

P.O. Anikeeva, C.F. Madigan, J.E. Halpert, M.G. Bawendi, V. Bulović
Sponsorship: ISN, MIT NSF MRSEC, PECASE

Hybrid light-emitting devices (LEDs), consisting of organic charge transporting layers and colloidal quantum-dot (QD) emissive layers [1], exhibit narrow electroluminescence (EL) spectra, characteristic of colloidal QD luminescence. The manifested saturated color emission is particularly desirable in flat-panel display applications and is broadly applicable to other technologies requiring high spectral quality lighting. The development of novel QD deposition techniques such as microcontact printing [2] allowed us to experimentally investigate the mechanisms of QD-LED operation by varying the position of the emitting QD monolayer within the stacked organic structure. We find that imbedding the emissive QD monolayer into the hole-transporting layer <10 nm away from the interface between hole and electron-transporting layers, improves the quantum efficiency of the device by >50%, while maintaining QD-LED spectral purity (Figure 1). These findings and additional experiments led us to the conclusion that maximizing exciton generation on organic molecules and subsequent energy transfer to QDs, while minimizing QD charging with electrons, improves QD-LED performance.

In order to verify our conclusions based on the previous experimental observations, we built a theoretical model for charge and exciton transport in organic LEDs (OLEDs) and QD-LEDs. Considering carrier drift and diffusion, we numerically simulate carrier concentration and electric field profiles in device structures; based on them, we calculate exciton concentration profiles (Figure 2). We find that the results of our model are in qualitative agreement with experimental data. We find that exciton diffusion and non-radiative energy transfer from organic thin films to QDs lead to maximum exciton concentration on QD sites, resulting in QD-LED spectra dominated by QD emission. We find that imbedding QDs into the TPD hole-transporting layer reduces electron concentration at QD sites and consequently eliminates QD luminescence quenching. It also reduces the electric field across the QDs, eliminating exciton dissociation.

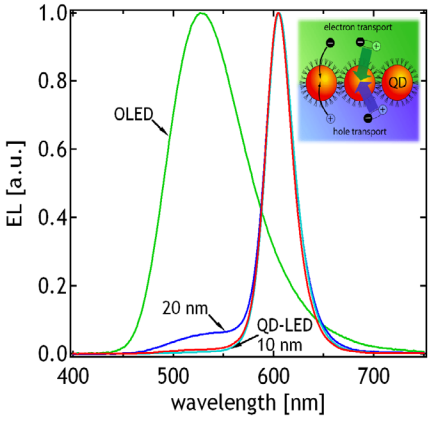

▲ Figure 1: Normalized EL spectra of OLED, QD-LEDs with QDs at the TPD/Alq_3 interface, QDs imbedded into TPD 10 nm and 20 nm below the interface. Inset: Schematic diagram of the charge injection and energy transfer from organic charge transporting layers to a monolayer of colloidal QDs.

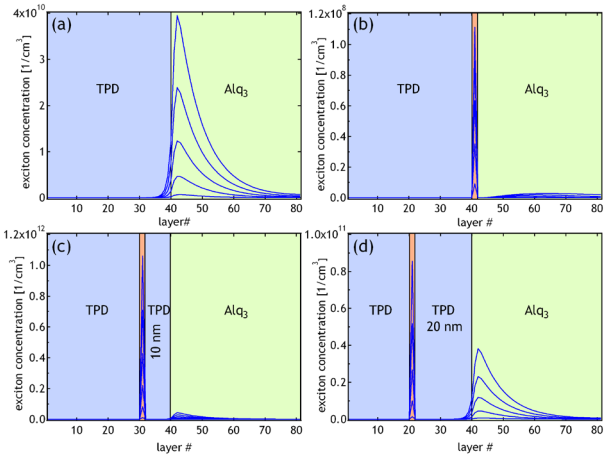

▲ Figure 2: Exciton concentration profiles obtained from numerical simulations. (a) OLED, (b) QD-LED with QDs at the TPD/Alq3 interface, (c) and (d) QDs imbedded into TPD 10 nm and 20 nm away from the interface. Theoretical exciton profiles are in qualitative agreement with experimental EL spectra shown in Figure 1.

References

[1] S.A. Coe-Sullivan, "Hybrid organic/quantum dot thin film structures and devices," Ph.D. thesis, Massachusetts Institute of Technology, Cambridge, 2005.
[2] L. Kim, "Deposition of colloidal quantum dots by microcontact printing for LED display technology," M.Eng. thesis, Massachusetts Institute of Technology, Cambridge, 2006.

Cathode Metal Diffusion and Doping in Organic Light-emitting Devices

P. Jadhav, B. Limketkai, M. Baldo
Sponsorship: DuPont-MIT alliance

Organic semiconductors employed in organic light-emitting devices (OLEDs) are typically assumed to be intrinsic. There are suggestions, however, that organic semiconductors may actually be doped within OLEDs [1]. It is important to resolve the origin of the apparent doping phenomenon because: (i) doping apparently determines the operating voltage and quantum efficiency, and (ii) compositional control is a prerequisite for the rational design of stable OLEDs. Indeed, one notable characteristic – the retained negative charge in tris(8-hydroxyquinoline) aluminum (AlQ_3)-based OLEDs -- has been directly correlated to degradation [1]. The retained charge undergoes a transition from negative to positive that is linearly related to the loss of luminance.

We demonstrate that one significant origin of impurities is cathode metal diffusion. Cathode materials diffuse into the bulk of the AlQ_3, introducing free charges if the cathode material reacts with neighboring AlQ_3 molecules. In addition, the presence of reactive cathode materials stabilizes electrons on other nearby AlQ_3 molecules, forming electron traps. Thus, the diffusion of cathode species is associated with both free charge and traps in AlQ_3. We probe charge stored in electron traps using capacitance-voltage[2]. In bilayer OLEDs consisting of AlQ_3 and a hole transport layer (HTL), holes are confined at the AlQ_3/HTL interface. Thus, the capacitance is determined by the thickness of the AlQ_3. Under reverse bias, the holes are extracted and the capacitance is determined by the thickness of the entire OLED (Figure 1). In the absence of stored charge, the transition in the observed capacitance should occur at the built-in potential, V_{BI}. But we observe transitions at more negative potentials, confirming the presence of fixed negative charge. The negative charge density calculated from these measurements decreases with cathode distance from the interface (Figure 2) and exhibits a clear dependence on the cathode material, confirming that the cathode is the origin of the fixed charge.

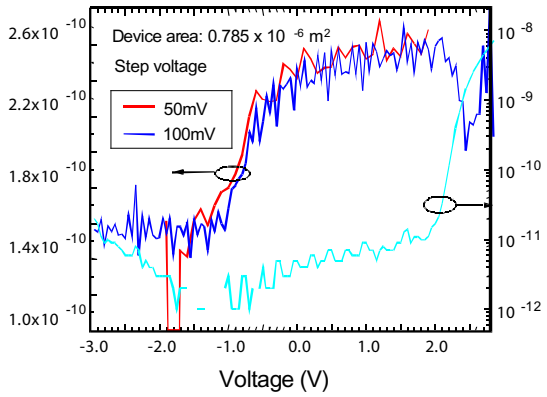

▲ Figure 1: Quasi-static capacitance-voltage measurement for a hetero-layer AlQ_3/HTL device. As the biasing voltage is reduced from forward to reverse bias, the capacitance changes from C_{AlQ3} to that of the series sum of C_{AlQ3} and C_{HTL}. This transition would be expected to occur at $V = V_{BI}$, which is the difference in work functions of the two electrodes. Instead, it occurs at a voltage further into reverse bias, revealing the existence of trapped negative charge in the AlQ_3 layer.

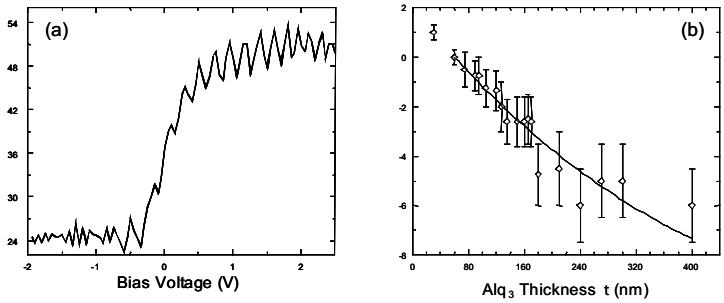

▲ Figure 2: The thickness dependence of the capacitive transition voltage. It is fit by a model assuming that the fixed charge density decreases exponentially with distance from the cathode.

References

[1] D.Y. Kondakov, W.C. Lenhart, and W.F. Nichols, "Operational degradation of organic light-emitting diodes: Mechanism and identification of chemical products," *Journal of Applied Physics*, vol. 101, no. 2, p. 24512, Jan. 2007.

[2] S. Berleb, W. Brutting, and G. Paasch, "Interfacial charges in organic hetero-layer light emitting diodes probed by capacitance-voltage measurements," *Synthetic Metals*, vol. 122, no. 1, pp. 37-39, May 2001.

The Density of States in Thin-Film Copper Phthalocyanine (CuPC) as Measured by Alternating Current Kelvin Probe Force Microscopy (AC-KPFM)

K. Celebi, K. Milaninia, P. Jadhav, M.A. Baldo

Sponsorship: DuPont-MIT alliance

The rational design of organic electronic devices is presently complicated by our inability to directly measure the energetic disorder in the semiconductor. Consequently, many studies have sought to obtain the density of states (DOS) in organic semiconductors. Unfortunately, existing techniques such as ultraviolet photoelectron spectroscopy or thermally stimulated luminescence either lack sufficient resolution or require complicated models for interpretation. The KPFM technique can measure DOS at a resolution of at least 1:1000. We improve upon the original KPFM technique of Tal *et al.* [1] and investigate its limitations. We employ alternating current (AC-KPFM) to reduce noise, and we minimize hysteresis due to charge trapping at the semiconductor/insulator interface. Finally, we model space charge phenomena that distort the data and we demonstrate that the AC-KPFM technique is applicable beyond the low inversion density regime analyzed by Tal *et al.*

Kelvin probe force microscopy (KPFM) employs a scanning probe to measure the local surface potential difference between the probe tip and a substrate. We perform the measurements on CuPC (hole transporter) organic thin-film transistors (OTFT). The source and drain are grounded to maintain equilibrium and a constant Fermi level in the channel. Then, the gate voltage is modulated, shifting the energy levels in the semiconductor. If the DOS at the Fermi level changes, the charge density in the channel must also change. Measurements of the surface potential detect this charging and in turn detect the DOS.

Devices were made with and without octadecyltrichlorosilane (OTS) passivation of the oxide surface. Consistent with previous observations, the magnitude of the threshold voltage was significantly reduced by OTS passivation. The OTS treatment also substantially reduces hysteresis, suggesting that passivation of the oxide surface reduces the trap density at the SiO_2-CuPC interface.

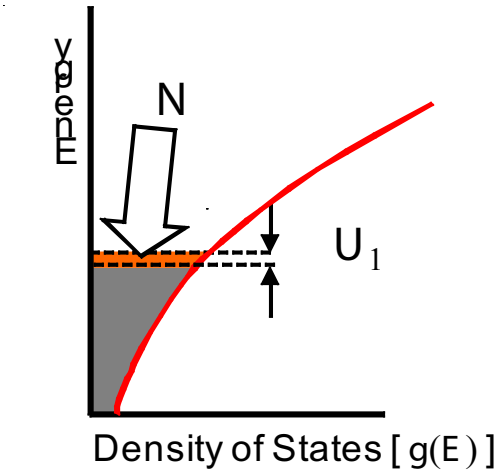

▲ Figure 1: Changes in the charge density in the channel change the surface potential *U* by an amount determined by the density of states.

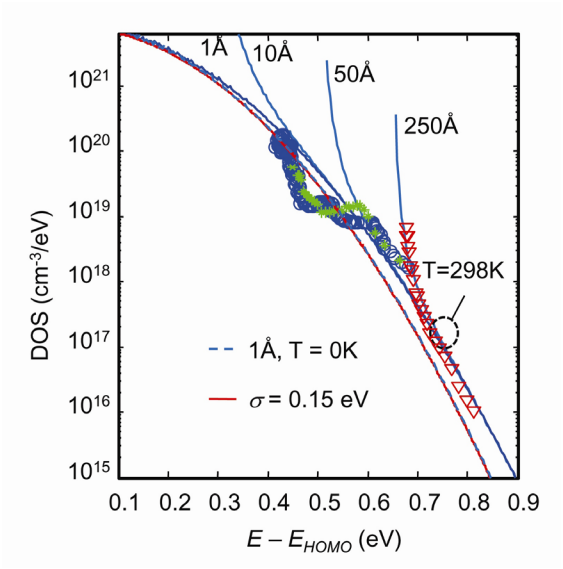

▲ Figure 2: The density of states calculated from AC and/or DC measurements on OTFTs of various thicknesses. The sharp increase in the DOS is due to the screening effect of accumulated charge. The solid lines are the result of simulations for a Gaussian density of states for films of the thicknesses shown.

Reference

[1] O. Tal, Y. Rosenwaks, Y. Preezant, N. Tessler, C.K. Chan, and A. Kahn, "Direct determination of the hole density of states inundoped and doped amorphous organic films with high lateral resolution," *Physical Review Letters*, vol. 95, no. 25, pp. 256405, Dec. 2005..

Heterojunction Photovoltaics Using Printed Colloidal Quantum Dots as the Photosensitive Layer

A.C. Arango, D.C. Oertel, M.G. Bawendi, V. Bulović
Sponsorship: ISN

Colloidal quantum dot (QD) systems offer distinct optical and electronic properties that are not easily attained by other nanostructured semiconductors, such as highly saturated emission in QD light-emitting-diodes, access to infrared radiation in QD photodetectors, and the prospect of optically optimized solar cell structures [1]. The prevailing deposition method for colloidal QD systems is spin casting, which introduces limitations such as solvent incompatibility with underlying films and the inability to pattern side-by-side pixels for multispectral photodetector arrays. In the present work we employ a non-destructive microcontact printing method, which allows for deposition of a thin quantum dot films onto a wide-band-gap organic hole transport layer, N,N'-Bis (3-methylphenyl)-N,N'-bis-(phenyl)-9,9-spiro-bifluorene (spiro-TPD), thus producing an inorganic/organic heterojunction that serves to enhance charge separation in the device. The top and bottom contacts are provided by ITO electrodes, allowing for near-transparency.

The performance of nanostructured devices is often critically dependent on the morphology of the constituent films in the device. Deposition of thin QD films from solution can result in rough and incomplete layers if the surface energy of the solvent is not well matched with the surface energy of the substrate. For instance, the low surface energy of a polydimethylsiloxane (PDMS) printing stamp must be modified to match the higher surface energy of the QD solvent in order to print smooth and complete QD films. When a layer of parylene-C is deposited on the PDMS stamp, a smooth and complete QD film can be printed, unlike the process in which a film is printed from a bare PDMS stamp (Figure 1). The device with a smooth and complete film yields superior performance, achieving a built-in potential (Vbi) of 1.46V for a QD band gap of 1.97eV (Figure 2). The Vbi is 74% of the band gap, one of the highest values achieved for photovoltaics of any kind. The present focus is on improving the device's performance and optimizing the photodetection response in the 1-μm to 2-μm wavelength region by utilizing different QD film chemistries.

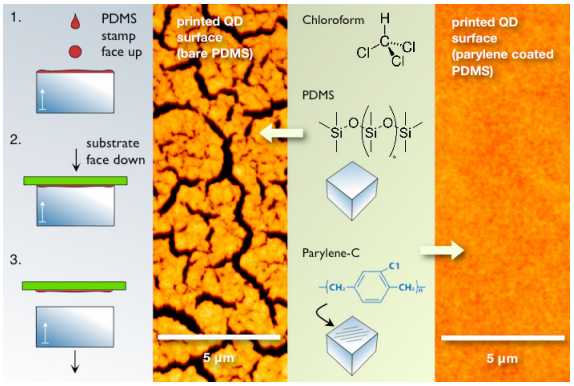

▲ Figure 1: Printing process (far left) and AFM images of QDs deposited from bare PDMS (left) and parylene coated PDMS (right). The QD solution is spin cast onto the PDMS stamp (1) and allowed to dry under vacuum for 30 minutes; then the substrate is placed on the stamp (2) and released (3). Chloroform has less of a surface energy mismatch with parylene than with PDMS, resulting in improved wetting. Smooth and continuous QD films are achieved down to a thickness of one monolayer.

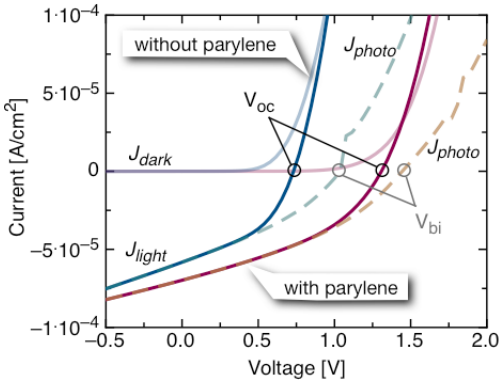

▲ Figure 2: Current-voltage characteristics for a photovoltaic device consisting of a QD film printed from a bare PDMS stamp (blue) and a parylene coated PDMS stamp (red). The short circuit current and the open circuit voltage (Voc) are improved for the QD device deposited from parylene. The built-in potential (Vbi) (the potential at which the current in light, Jlight, is equal and opposite to the current in dark, Jdark) reaches 1.46V.

Reference

[1] D.C. Oertel, M.G. Bawendi, A.C. Arango, and V. Bulović, "Photodetectors based on treated CdSe quantum-dot films," *Applied Physics Letters*, vol. 87, no. 21, p. 213505, Nov 2005.

Organic/Quantum-dot Photoconductor

T. Osedach, J. Ho, A. Arango, S. Geyer, M. Bawendi, V. Bulović
Sponsorship: ISN, CMSE

We demonstrate an organic/quantum-dot (QD) photodetector in which charge transport is governed by a single organic layer and the optical absorption can be tuned according to quantum confinement of QDs composing a second layer. The optical and electrical characteristics of the device can be optimized independently through the modification of these two layers. A similar device composed of organic materials was previously demonstrated by our group [1]. Our work stands in contrast to the operation of conventional layered organic photodetectors in which carriers generated at a dissociating interface must travel through both heterojunction materials to reach the opposite electrodes. In such a device both layers are crucial to charge transport, making it difficult to modify the optical properties of the device, such as absorption spectrum, without significantly affecting its electrical characteristics.

The device consists of metallic interdigitated electrodes over which an organic charge transport layer is thermally evaporated (see Figure 1). Microcontact printing is then used to deposit a 50-nm-thick layer of colloidal QDs, completing the structure. The organic/QD interface manifests a type-II heterojunction suitable for dissociating excitons. Under illumination, light is absorbed throughout both layers of the device. Excitons created within an exciton diffusion length of the heterojunction interface are dissociated there, increasing in the carrier concentrations of both layers. A bias corresponding to a field of ~10^4 V/cm is applied across the electrodes to facilitate carrier collection. The increased hole density increases the organic film conductivity, which in turn manifests an increase in lateral current through the device. Figure 2 shows spectra of the external quantum efficiency exhibiting high efficiencies attributable to quantum-dot absorption. The device clearly separates the photogeneration and charge transport mechanisms and as such serves as a unique platform for studies of charge transfer at organic/QD interfaces for QD-sensitized photoactive devices.

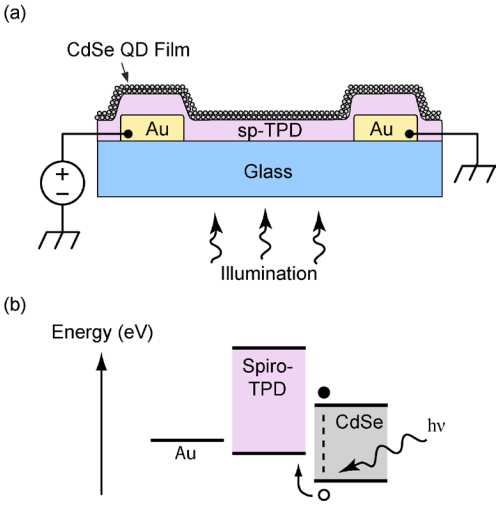

▲ Figure 1: (a) Schematic of the device structure. (b) Energy band diagram. Excitons dissociate at the interface between the organic film and the quantum dots.

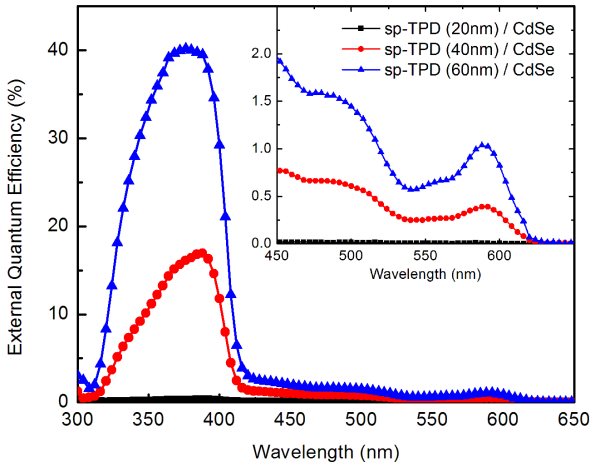

▲ Figure 2: External quantum efficiency spectrum. High efficiencies have been measured at absorption peaks corresponding to the organic layer as well as to the quantum-dot layer.

Reference

[1] J. Ho, A. Arango, and V. Bulović, "Lateral organic bi-layer heterojunction photoconductors," *Applied Physics Letters*, to be published.

Organic Multi-layer Lateral Heterojunction Phototransistors

J.C. Ho, J.A. Rowehl, V. Bulović
Sponsorship: ISN, CMSE

We fabricate a two-terminal, lateral multi-layer phototransistor [1] consisting of three molecular organic thin films with cascading energy bands (see Figure 1a): the charge transport layer is (CTL), N,N'-bis(3-methylphenyl)-N,N'-diphenyl-1,1'-biphenyl-4,4'-diamine (TPD); the charge spacer layer (CSL), tris(8-hydroxyquinoline)alumi num(III) (Alq_3); and the exciton generation layer (EGL), 3,4,9,10-perylenetetracarboxylic bis-benzimidazole (PTCBI). Placing an interstitial spacer layer between the CTL and the EGL improves the external quantum efficiency of tri-layer phototransistors over bi-layer, Type-II heterojunction phototransistors.

Light excitation acts as a pseudo "gate electrode" by generating excitons in PTCBI (EGL). Those excitons diffuse to the PTCBI/Alq_3 interface where they dissociate, leaving the electron behind in PTCBI, while the hole is initially injected into Alq_3 from where it can transfer to the more energetically favorable states in TPD. Excess holes in the TPD film raise the hole carrier concentration in the TPD film and increase the device conductance by forming a channel of excess carriers at the TPD/Alq_3 interface. The thin film of Alq_3 (CSL), between TPD (CTL) and PTCBI (EGL), spatially separates the dissociated carriers, reducing the likelihood of bimolecular recombination across the TPD/PTCBI interface. Bi-layer heterojunction phototransistors consisting of TPD and PTCBI alone have been shown to improve the external quantum efficiency over single layers of TPD and PTCBI by several orders of magnitude [2]. By introducing a CSL in a lateral tri-layer arrangement, we demonstrate an order of magnitude improvement over bi-layer lateral phototransistors without a CSL (see Figure 1b). The phototransistor contacts consist of interdigitated gold fingers that form a 30-mm-wide, 10-μm-long serpentine channel. Measurement of the photocurrent from a biased multi-layer, lateral heterojunction device [Au/TPD(47.5 ± 2) nm/Alq_3(6.2 ± 2) nm/PTCBI(52.5 ± 2) nm] reveals an internal quantum efficiency of (16 ± 1)% at an optical excitation wavelength of 573 nm. A thickness study of the Alq_3 spacer layer experimentally demonstrates the dependence of the carrier lifetime (at a heterointerface) and photoresponse efficiency on the spatial separation of dissociated charge.

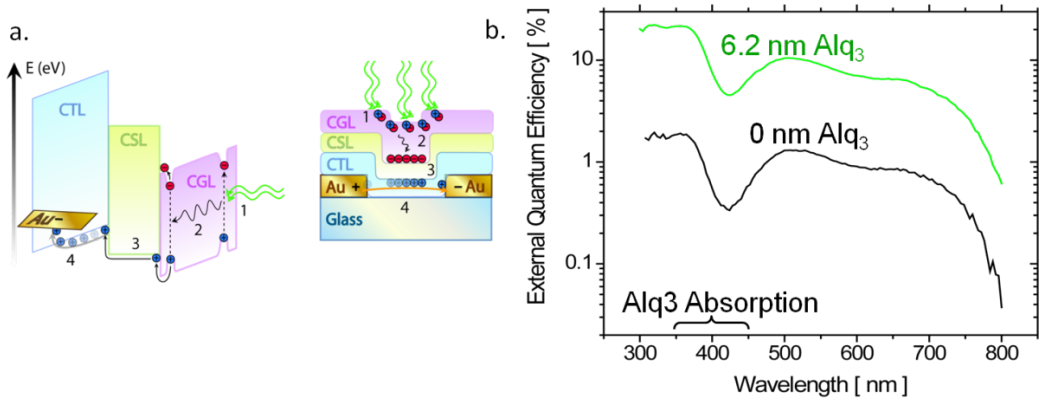

▶ Figure 1: a. Energy band/cross-sectional diagrams of tri-layer phototransistors (1. absorption , 2. exciton diffusion, 3. exciton dissociation, 4. charge transport) b. Spectral response of EQE showing benefit of CSL .

References

[1] J. Ho, J. Rowehl, and V. Bulović, "Organic multi-layer lateral heterojunction phototransistors," to be presented at *Electronic Materials Conference*, Santa Barbara, CA, June 2008.

[2] J. Ho, A. Arango, and V. Bulović, "Lateral organic bi-layer heterojunction photoconductors," *Applied Physics Letters*, June 2008, to be published.

Inkjet Printing of P3HT/PCBM Solar Cells

T. Osedach, A. Arango, J. Chen, V. Bulović
Sponsorship: ISN, CMSE

Polymeric solar cells offer the promise of a low-cost alternative to conventional inorganic photovoltaic devices. Particularly encouraging are solar cells consisting of blends of the polymer poly(3-hexylthiophene) (P3HT) and the fullerene derivative [6,6]-phenyl-C61-butyric acid methyl ester (PCBM) sandwiched between electrodes (see Figure 1). Recently, power efficiencies as high as 5.2% have been reported [1]. In an attempt to further improve the performance and cost-effectiveness of these solar cells so that they may become a more viable technology, we are exploring a number of variations to the standard processing procedure to fabricate them.

Presently, the processing of P3HT:PCBM devices used by most other groups involves a combination of spin-coating and thermal evaporation steps that are limited to small substrate sizes. In our study, we have used inkjet printing, a low-cost and highly scalable deposition technique, to deposit the active layers in P3HT:PCBM solar cells. The deposition of metal electrodes with inkjet printing is also currently being explored. Figure 2 shows current-voltage characteristics of a printed solar and a control device with a spin-coated active layer. The short-circuit current of the printed solar cell in this case exceeds that of the control device.

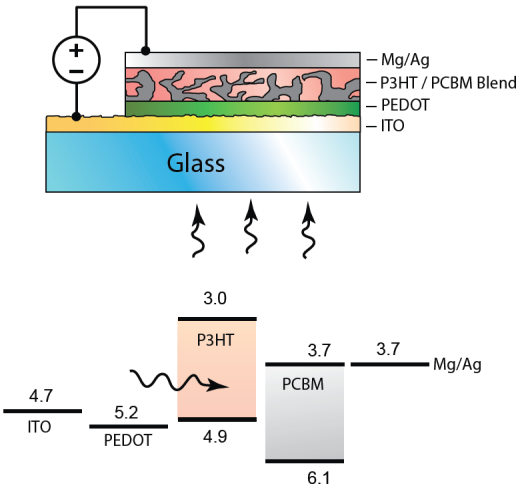

▲ Figure 1: (top) Device structure of a P3HT:PCBM solar cell. (bottom) Energy band diagram of the device. The P3HT and PCBM create a type-II heterojunction suitable for separating excitons.

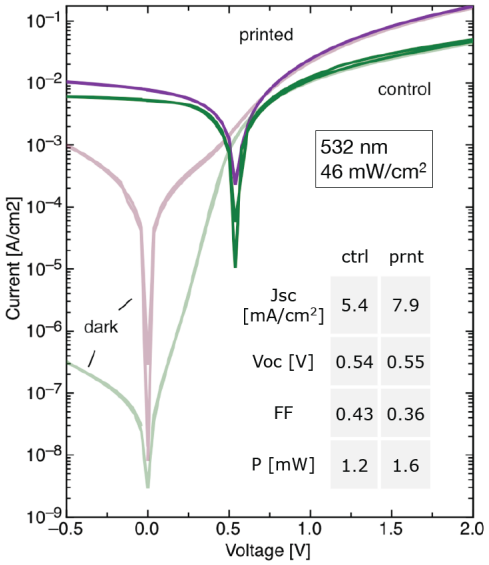

▲ Figure 2: Current-voltage characteristics of an inkjet-printed solar cell versus a control device fabricated using spin-casting. The printed device exhibits a superior short-circuit current and open-circuit voltage, but a higher dark current.

Reference

[1] M.D. Irwin, D.B. Buchholz, A.W. Hains, R.P.H. Chang, and T.J. Marks, "P-type semiconducting nickel oxide as an efficiency-enhancing anode interfacial layer in polymer bulk-heterojunction solar cells," *Proc. National Academy of Sciences*, vol. 105, pp. 2783-2787, 2008.

Monochromatic Organic Solar Cells

T.D. Heidel, M.A. Baldo
Sponsorship: DOE

With a theoretical efficiency similar to conventional inorganic photovoltaics (PV) and the potential to be manufactured inexpensively over large areas, organic semiconductor technology offers a promising route to ubiquitous solar energy generation [1]. However, organic PVs are constrained by a tradeoff between exciton diffusion and optical absorption: as absorption is increased by fabricating thicker devices, the efficiency of charge separation decreases since excitons cannot reach the charge separation interface. Ultimately, this tradeoff limits the portion of the solar spectrum that optimized organic PVs can harness.

In our work, we increase absorption in organic solar cells within the limits of exciton diffusion by fabricating cells inside a resonant microcavity [2]. As Figure 1 illustrates, the resonant cavity devices have a semi-reflecting bottom contact and a fully reflecting mirror contact on the back. The layers between the contacts consist of a transparent optical spacing layer and a thin organic solar cell [3]. Modulating the thickness of the transparent spacing layer allows the increase in absorption to be tuned across the entire visible spectrum. The reflectivity of the contacts can also be engineered to modulate the width of the absorption resonance. Fabricating a thin organic solar cell within the cavity allows charge separation efficiencies to reach 100%. Modeling indicates that absorption in the organic semiconductor layers can be increased as much as 91% relative to absorption in optimized organic PVs with no resonant cavity; see Figure 2.

Resonant cavity monochromatic organic solar cells have applications in tandem organic solar cells and advanced solar concentrator designs. Organic tandem solar cells attempt to overcome the tradeoff between exciton diffusion and absorption by utilizing multiple heterojunctions that absorb most strongly in different regions of the solar spectrum. High-efficiency, monochromatic solar cells could increase the efficiency of these individual multiple heterojunctions. The efficiency of many solar concentrator designs could also be maximized by using solar cells optimized for specific regions of the solar spectrum.

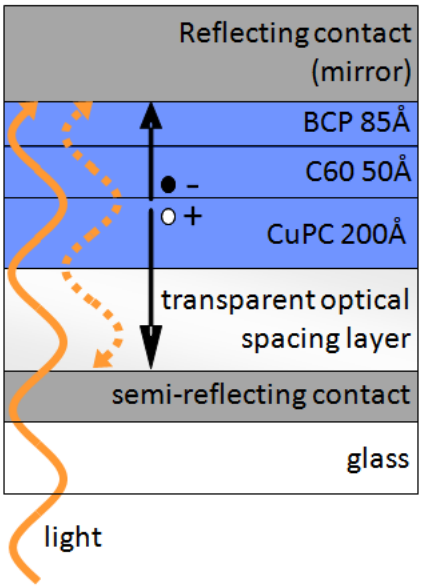

▲ Figure 1: Resonant cavity organic solar cells consist of a thin organic PV and transparent optical spacing layer fabricated between reflecting contacts.

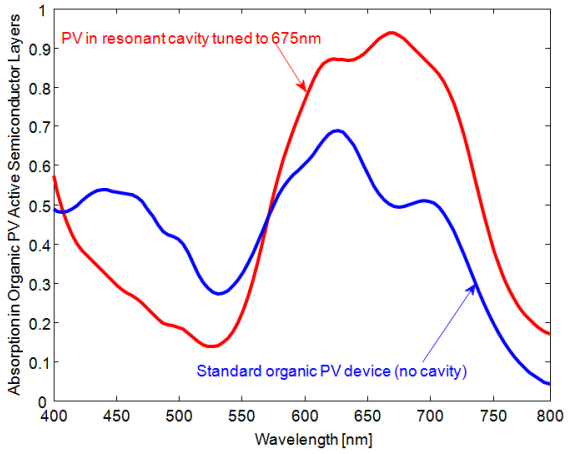

▲ Figure 2: The resonant cavity enhances absorption strongly in one region of the solar spectrum. The absorption peak can be tuned across the entire visible spectrum. Combining two or more cavity organic PVs will allow for enhancement across the entire visible spectrum.

References

[1] P. Peumans, A. Yakimov, and S.R. Forrest, "Small molecular weight organic thin-film photodetectors and solar cells," *Journal of Applied Physics*, vol. 93, no. 7, pp. 3693-3723, Apr. 2003.

[2] T.D. Heidel, J.K. Mapel, M. Singh, K. Celebi, and M.A. Baldo, "Surface plasmon polariton mediated energy transfer in organic photovoltaic devices," *Applied Physics Letters*, vol. 91, no. 093506, Aug. 2007.

[3] K. Walzer, B. Maennig, M. Pfeiffer, and K. Leo, "Highly efficient organic devices based on electrically doped transport layers," *Chemical Reviews*, vol. 107, pp. 1233-1271, Mar. 2007.

Charge Recombination in Small-molecular-weight Organic Solar Cells

J. Lee, M. Segal, M.A. Baldo
Sponsorship: SRC/FCRP MSD

Organic solar cells promise efficient and cost-effective solar energy generation from low-cost materials and a low-temperature manufacturing process compatible with flexible plastic substrates. In organic photovoltaic cells, photon absorption creates a bound electron-hole pair, or exciton. The excitons diffuse toward the donor-acceptor (DA) heterojunction. The energy offset at the DA interface dissociates the strongly bound excitons in organic molecules with near-unity efficiency. Excitons are separated into charge transfer (CT) states, which are bound electron-hole pairs across the DA junction [1]. The CT states can be dissociated into free carriers that ultimately generate photocurrent or they may recombine into low-energy states such as ground states or triplet excitons. The recombination of CT states can cause a substantial loss in the photovoltaic efficiency depending on the CT state lifetime and the operating voltage bias.

We perform transient absorption spectroscopy to study the charge recombination dynamics of small-molecular-weight organic solar cells. The transient absorption setup was built as illustrated in Figure 1. The samples are held at the temperature of 50K. We investigate thin film bulk heterojunction of the archetype organic solar cell molecules, copper phthalocyanine (CuPC) and 3,4,9,10-perylenetetracarboxylic bis-benzimidazole (PTCBI). To assign the absorption wavelength of CuPC cations and PTCBI anions, the photoinduced absorption (PIA) spectra of related organic molecules are compared as shown in Figure 2. The CT states in CuPC/PTCBI live up to milliseconds. Also, we found that the states featuring the broad peak at 1450 nm decay much faster than the CT states with the lifetime of ~150 μs. We tentatively assign the state at 1450nm to the PTCBI triplet exciton. The evidence of triplet excitons implies that PTCBI triplet formation is an importance source of recombination loss in CuPC/PTCBI photovoltaic cells.

Further study of organic heterojunction thin films is expected to reveal the physical origin of charge recombination and should contribute to reducing the recombination loss in organic photovoltaic cells.

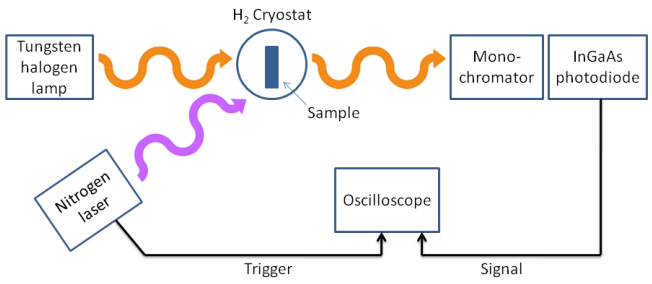

▲ Figure 1: Schematic diagram of the transient absorption setup. The nitrogen laser creates excitons, which we subsequently dissociated into CT states. Then, the CT states absorb the white light provided by the tungsten halogen lamp. The photodiode detects the change of the transmitted light at the selected wavelength. The setup probes the decay dynamics of CT states.

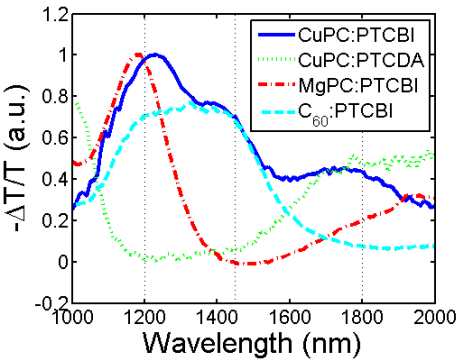

▲ Figure 2: The PIA spectrum of organic bulk heterojunction thin films that are studied in this work. PTCDA: 3,4,9,10-perylenetetracarboxylic dianhydride, MgPC: magnesium phthalocyanine.

Reference

[1] P. Peumans, A. Yakimov, and S.R. Forrest, "Small molecular weight organic thin-film photodetectors and solar cells," *Journal of Applied Physics*, vol. 93, no. 7, pp. 3693-3723, Apr. 2003.

High-efficiency Organic Solar Concentrators

J.K. Mapel, M.J. Currie, T.D. Heidel, S. Goffri, M.A. Baldo
Sponsorship: DOE, NSF NIRT

Organic solar concentrators (OSC) are a class of luminescent solar concentrators [1] that exploit advances in thin-film organic semiconductor technology and low-cost manufacturing processes to create efficient, large-area optical concentrators for inorganic solar cells. The OSCs are dye-based light concentrators that operate through successive absorption and emission of light into confined modes of a light guide to a photovoltaic cell for electrical conversion; see Figure 1. These OSCs hold the potential to reduce the cost per generated watt of power for solar power transduction systems by separating the optical and electrical parts of a solar cell. Previous demonstrations have shown limited performance due to the high probability of re-absorption of confined light, which lowers the guided transport efficiency [2].

We have fabricated single and tandem waveguide organic solar concentrators with quantum efficiencies exceeding 50% and projected power efficiencies up to 6.8%; see Figure 2. Near field energy transfer [3], solid state solvation [4], and phosphorescence [5] are employed within a thin-film organic coating on glass to substantially reduce self-absorption losses, enabling flux gains exceeding F = 10, meaning that a photovoltaic cell attached to the concentrator generates approximately 10 × the power of the photovoltaic cell without optical concentration. Flux gains of F > 10 in organic solar concentrators should enable the economical use of high performance photovoltaic cells in low-cost systems.

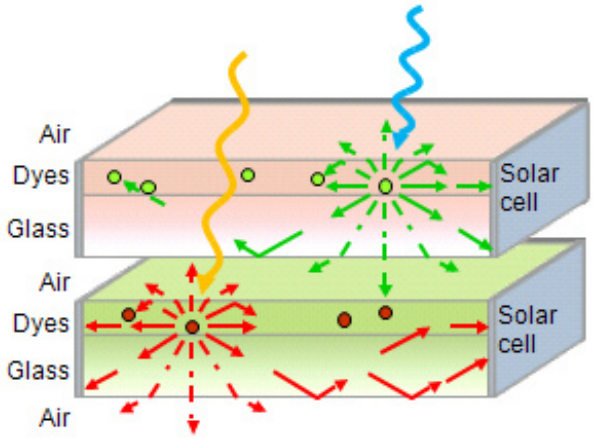

▲ Figure 1: Physical processes leading to energy conversion in an OSC. Photons are absorbed by a luminescent chromophore embedded within or coating a waveguide. The chromophore can re-radiate a photon of equal or lesser energy, and some portion of the emitted radiation will be confined in the waveguide by total internal reflection. Some fraction of the trapped light will travel to another face of the guide that has a smaller cross-sectional area, where a photovoltaic element resides for the collection of the concentrated light.

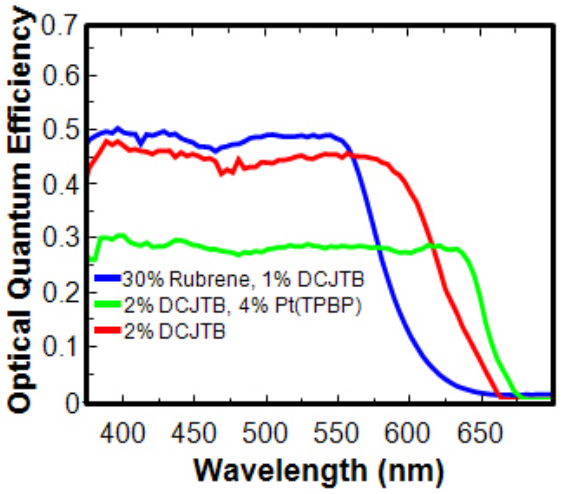

▲ Figure 2: Optical quantum efficiency (OQE) spectra at a geometric gain of 3. The OQE is the fraction of incident photons that are emitted from the edges of the single waveguide OSC. In blue, the OSC utilizes near-field energy transfer from the AlQ3 matrix and rubrene dopants to pump emission through DCJTB, a laser dye. In green, light is absorbed by AlQ3, rubrene, and Pt(TBTP) and phosphoresces from Pt(TBTP). The energetic separation between absorption and emission in these OSCs enables higher flux gains than in single-material systems.

References

[1] W.H. Weber and J. Lambe, "Luminescent greenhouse collector for solar radiation," *Applied Optics*, vol. 15, p. 2299, 1976.
[2] J.S. Batchelder, A.H. Zewail, and T. Cole, "Luminescent solar collectors: experimental and theoretical analysis of their possible efficiencies," *Applied Optics*, vol. 20, p. 3733, 1981.
[3] T. Förster, "Transfer mechanisms of electronic excitation," *Discussions of the Faraday Society*, vol. 27, p. 7, 1959.
[4] V. Bulović *et al.*, "Bright, saturated, red-to-yellow organic light-emitting devices based on polarization-induced spectral shifts," *Chemical Physics Letters*, vol. 287, p. 455, 1998.
[5] M.A. Baldo *et al.*, "Highly efficient phosphorescent emission from organic electroluminescent devices," *Nature*, vol. 395, p. 151, 1998.

Luminescent Solar Concentrators Employing Phycobilisomes

C.L. Mulder, L. Theogarajan, M. Currie, J.K. Mapel, M.A. Baldo
Sponsorship: NSF NIRT, DOE

We present luminescent solar concentrators (LSCs) employing phycobilisomes from cyanobacteria. Luminescent solar concentrators are non-tracking optical collectors that increase the effective light-capture area of a solar-energy conversion device, while reducing the size of the expensive photovoltaic (Figure 1a) [1]. The geometric gain, *G*, is an important metric of LSC performance. It is defined as the ratio of the light collection area to that of the photovoltaic. Increasing *G* increases the total power per unit cost. But at large geometric gains, photons trapped in the LSC are subject to self-absorption losses that degrade performance. In this work we employ a biological photosynthetic system to study and circumvent the effects of self-absorption.

Phycobilisomes are macromolecular antenna complexes that are responsible for collecting light in photosynthetic systems (see Figure 2b for a schematic representation) [2]. Each of these proteins serves as a scaffold for pigment molecules, also known as chromophores. The chromophores are arranged through self-assembly in cascading Förster energy transfer pathways that couple short wavelength chromophores at the extremities of the complex to long wavelength chromophores at the core of the complex, thereby enhancing the Stokes shift between absorption and emission. We have characterized the optical absorbance and photoluminescence spectra and efficiencies of several different types of phycobilisomes and compared their performance when used as the active dye in a liquid or solid state LSC. The first type of phycobilisomes consisted of allophycocyanin (APC) with short rods of phycocyanin (PC) proteins (green). The second type consisted of APC with long rods of PC and PE proteins (red), which showed an increased Stokes shift in comparison to the first type of phycobilisomes. This increase in rod length was accompanied by a better performance with geometric scaling, reflecting the suppression of self-absorbance losses achieved by reducing the overlap between the emission and absorption spectra. When the internal Förster energy transfer was shut off by breaking up the phycobilisomes into their loose protein complexes, the LSC showed an even larger drop in efficiency with increasing geometric gain (blue). At G =9.3, the efficiency was 50% lower in the broken complexes than the complete APC + PC + PE phycobilisomes. These results suggest that using resonant energy transfer from higher to lower energy chromophores might provide a route to reducing self-absorption losses in LSCs.

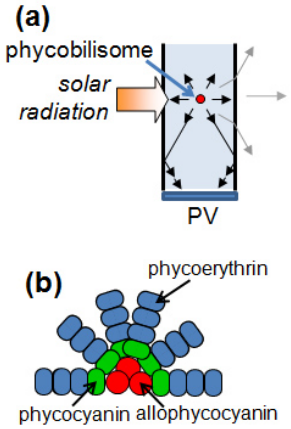

▲ Figure 1: (a) A schematic representation of a luminescent solar concentrator. (b) A schematic representation of a phycobilisome. These antenna complexes consist of a core of allophycocyanin (APC) that is connected to radial rods of phycocyanin (PC) billins and/or phycoerthyrin (PE) billins.

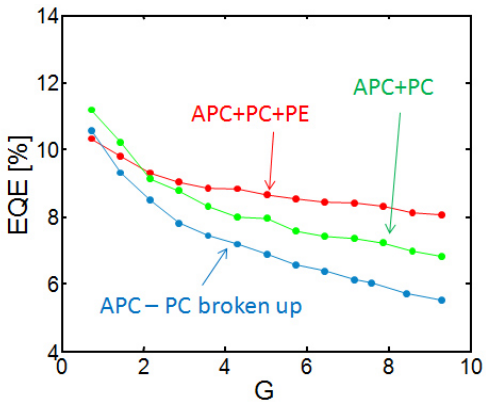

▲ Figure 2: External quantum efficiency at the peak absorption wavelength vs. geometric gain of LSCs employing phycobilisomes as the optical dye system. The complexes having the largest Stokes shift, the phycobilisomes with APC, PC and PE (red), showed the least roll-off with increasing G. The complexes with APC and short rods of PC exhibited a larger roll-off, while the dye system for which the internal Förster transfer was shut off (blue) had the poorest performance with increasing G.

References

[1] J.S. Batchelder, A.H. Zewail, and T. Cole, "Luminescent solar concentrators. 2: Experimental and theoretical analysis of their possible efficiencies," *Applied Optics*, vol. 20, pp. 3733-3754, Nov. 1981.

[2] R.E. Blankenship, *Molecular Mechanics of Photosynthesis*. Oxford: Blackwell Science Ltd., 2002.

Solution-processed Organic Solar Concentrators

S. Goffri, M. Currie, J. Mapel, M.A. Baldo

Solar energy is a clean and abundant energy source that promises to provide sustainable and economical sources of renewable power. Solar power generation is growing; however, it is still more expensive than fossil-fuel-based electricity sources. To address the cost of solar power, we are developing organic solar concentrators (OSCs) as an alternative to conventional solar concentrators. These OSCs do not require tracking of the sun or cooling of the solar cells and they require a smaller area of photovoltaic (PV) cells for the same power output.

An OSC is composed of organic chromophores to absorb sunlight and re-emit photons into a planar waveguide with PV cells attached to the edges [1-4]. The performance of an OSC is largely limited by self-absorption of the emitted photons by organic chromophores due to an overlap between their absorption and emission. We have investigated the used of novel chromophores and their compositions to reduce the overlap between emission and absorption. We coat glass flat-plate collectors using solution-processing, resulting in low-cost, thin-film solar collectors. This enables us to use recent advances in organic optoelectronics and apply near-field energy transfer to reduce the required concentration and hence the self-absorption of the emissive dye [5] (Figure 1).

The ratio of the area of the concentrator to the area of the PV cell is the geometric gain, *G*. Figure 2 shows the external quantum efficiency (EQE) as a function of geometric gain for different systems measured at $\lambda = 489$ nm for the composite perylene-based fluorescent system compared to the conventional 4-(dicyanomethylene)-2-*t-butyl*-6-(1,1,7,7-tetramethyljulolidyl-9-enyl)-4*H*-pyran(16) (DCJTB)-based fluorescent system, measured at $\lambda = 532$ nm. The DCJTB-based OSC shows the strong self-absorption. The self-absorption is lower in the composite perylene-based OSC, consistent with the spectroscopic data in Figure 1.

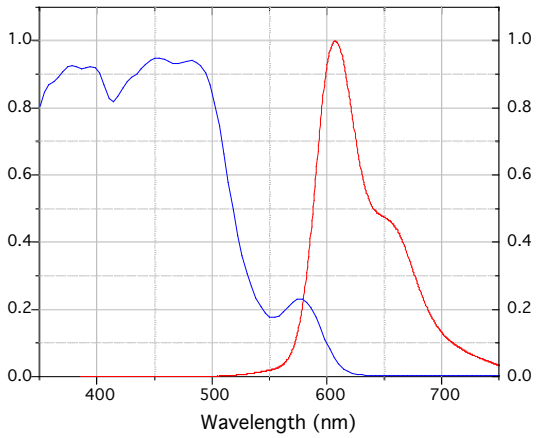

▲ Figure 1: Normalized absorption and emission spectra of perylene-based OSC film. The ratio between the peak absorption coefficient and the absorption coefficient at the emission wavelength provides a measure of the self-absorption in an OSC film.

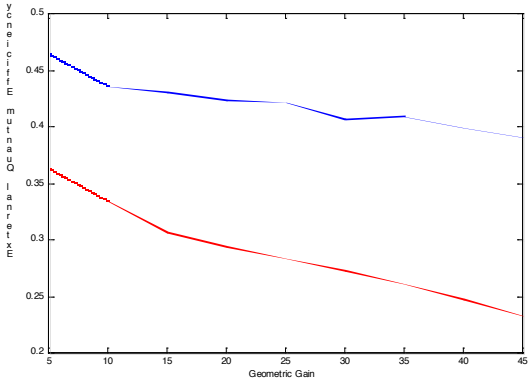

▲ Figure 2: OSC efficiency as a function of geometric gain, *G*. With increasing *G*, photons must take a longer path to the edge-attached PV, increasing the probability of self-absorption losses. Blue: perylene composite system, red: single DCJTB-based system.

References

[1] J.S. Batchelder, A.H. Zewail, and T.W. Cole, "Luminescent solar concentrators. 1: Theory of operation and techniques for performance evaluation," *Applied Optics*, vol. 18, pp. 3090-3110, Sept. 1979.

[2] J.S. Batchelder, A.H. Zewail, and T.W. Cole, "Luminescent solar concentrators. 2: Experimental and theoretical analysis of their possible efficiencies," *Applied Optics*, vol. 20, pp. 3733-3754, June 1981.

[3] A. Goetzberger and W. Greubel, "Solar energy conversion with fluorescent concentrators," *Applied Physics*, vol. 14, pp. Sep. 1977.

[4] W.H. Weber and J. Lambe, "Luminescent greenhouse collector for solar-radiation," *Applied Optics*, vol. 15, pp. 2299-2300, Oct. 1976.

[5] T. Förster, "Transfer mechanisms of electronic excitation," *Discussions of the Faraday Society*, vol. 27, pp. 7-17, Apr. 1959.

Self-absorption Measurements of Photoluminescent Efficiency of Thin-film Organic Semiconductors

Authors: M. Currie, J. Mapel, S. Goffri, M.A. Baldo
Sponsorship: DARPA/AFOSR, NSF NIRT

Characterizing the photoluminescent (PL) efficiency of thin films is essential to ascertaining the performance limits of light-emitting devices. The PL efficiency is the fraction of photons emitted per photon absorbed. Integrating sphere measurements is a common method used to measure PL efficiencies, but we show that the substrate must possess an index of refraction greater than that of the thin film to be valid [1-3]. The substrate index restriction is demonstrated by measuring the PL of commonly used organic materials on low- and high-index substrates. Measurements on low-index substrates exhibit optical losses due to thin-film waveguiding that result in an errors up to 50%. This effect is pronounced for low Stokes-shift films with large self-absorption. Figure 1 depicts the three light-paths for a thin film deposited on a transparent substrate, and Figure 2 shows the measurement set-up.

To illustrate substrate effects on PL measurements, three films were prepared on high (n = 1.80) and low (n = 1.52) index glass substrates that are 25mm x 25mm x 2mm in size. A neat 200-nm-thick film of tris (8-hydroxyquinoline) aluminum (AlQ_3), and a 200-nm-thick film of AlQ_3 and rubrene at (50% v/v) were thermally deposited. The PL efficiency of AlQ_3 is 29.2% and 28.1% on high- and low-index substrates, respectively. The error due to thin-film waveguiding on the low-index substrate is low due to the large Stokes shift and low self-absorption in AlQ3. The PL efficiency of rubrene, however, is 43.3% and 30.2% on high- and low-index substrates, respectively demonstrated a significant error if the PL efficiency measurement is performed on low-index substrates.

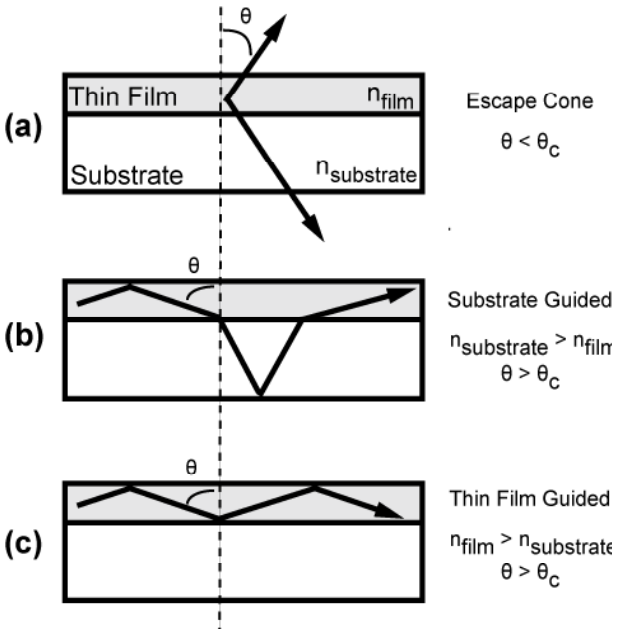

▲ Figure 1: Light-paths for a thin film on a transparent substrate: There are three potential pathways for light to travel within, and eventually leave, a thin film deposited on a transparent substrate: (a) escape cone light, (b) substrate-guided light, and (c) thin-film-guided light. Light that is guided in the thin film will largely be reabsorbed and underestimate PL in these measurements.

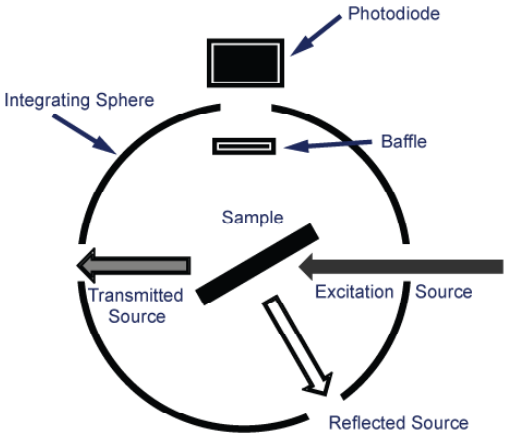

▲ Figure 2: Schematic of Integrating Sphere Measurement: Shown is the configuration used to measure PL within an integrating sphere. The sphere and sample are aligned such that the transmitted and reflected beams of the excitation source leave the sphere through an outlet port. The baffle within the integrating sphere prevents the photodiode from sensing direct photoluminescence from the sample.

References

[1] N.C. Greenham, N.C., I.D.W. Samuel, G.R. Hayes, R.T. Phillips, Y. Kessener, S.C. Moratti, et al., "Measurement of absolute photoluminescence quantum efficiencies in conjugated polymers," *Chemical Physics Letters*, vol. 241, pp. 89-96, 1995.

[2] A.R. Johnson, S.J. Lee, J. Klein, and J. Kanicki, "Absolute photoluminescence quantum efficiency measurement of light-emitting thin films," *Review of Scientific Instruments*, vol. 78, no. 9, pp. 096101:1-3, 2007.

[3] A. Nollau, M. Hoffmann, K. Floreck, T. Fritz, and K. Leo, "A simple measurement of the absolute internal quantum efficiency of thin organic films," *Journal of Applied Physics*, vol. 87, no. 11, pp. 7802-7804, 2000.

Radiative Spectrum Modification through Photonic Crystal-based Tungsten Microstructures

N. Jovanović, I. Čelanović, J. Kassakian

Sponsorship: Toyota Motor Corporation, MIT/Industry Consortium on Advanced Automotive Electrical/Electronic Components and Systems

This research investigates the fabrication, modeling, characterization, and application of tungsten two-dimensional (2D) photonic crystals (PhCs) as selective emitters and means of achieving higher efficiencies in thermophotovoltaic (TPV) energy conversion systems. A basic TPV system (Figure 1) consists of two parts: a thermal emitter and a photovoltaic (PV) diode. Thermal energy is provided to an emitting surface — the thermal emitter — which in turn radiates a spectrum of photons. The radiated photons are converted into free charge carriers when absorbed by the PV diode. Advantages of TPV systems include quiet operation, long lifetime, relatively low maintenance, portability, and scalability (TPV systems can be designed to meet a variety of energy needs, from watts to kilowatts). The two main shortcomings of TPV systems are low efficiency and high cost. The results of this research show that TPV systems can even exceed the efficiency of conventional power conversion mechanisms through highly-efficient spectral control.

Spectral control in TPV systems refers to the modification of the emitted spectrum to best match the PV diode sensitivity. In our particular case, spectral control is achieved through use of two components: a selective emitter and an optical filter. The optical filter, a result of our previous research project, is a one-dimensional dielectric stack [1] designed to match the gallium antimonide diode characteristics, which have become the standard in TPV systems. The selective emitter is a tungsten microstructure based on a 2D PhC pattern. Optical characterization of our selective emitter prototypes is found to be in excellent agreement with simulation and has provided an experimental confirmation of selective emitter performance (Figure 2). We show that selective emitters can substantially increase spectral efficiency, providing as much as three times the radiative power density of planar tungsten. Our measurements indicate as much as 94% combined spectral efficiency of a selective emitter and a dielectric stack mirror for TPV system applications.

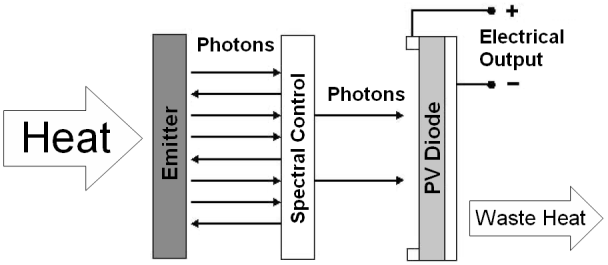

▲ Figure 1: A basic thermophotovoltaic power conversion system consists of an emitter and a photovoltaic diode. The addition of spectral control components drastically increases the system efficiency.

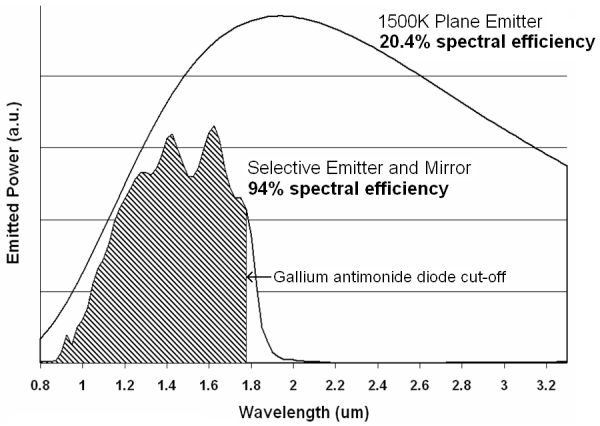

▲ Figure 2: Radiative spectrum of a tungsten PhC-based selective emitter prototype compared to a planar black-body emitter at 1500K. Used with gallium antimonide diodes, our selective emitter and dielectric filter achieve 94% spectral efficiency.

Reference

[1] F. O'Sullivan, I. Čelanović, N. Jovanović, and J. Kassakian, "Optical characteristics of one-dimensional Si/SiO2 photonic crystals for thermophotovoltaic applications," *Journal of Applied Physics*, vol. 97, Jan. 2005.

Packaging Superconductive Nanowire Single-photon Detectors

X. Hu, K.K. Berggren, F.N.C. Wong
Sponsorship: IARPA

The superconductive nanowire single-photon detector (SNSPD) is an emerging ultra-sensitive photon-counting technology that can be used in quantum key distribution, deep-space optical communication and defect-detection for integrated circuits. In the past, we have successfully developed a robust process to fabricate SNSPDs and have demonstrated device-detection efficiency above 50% at near-infrared wavelengths [1]. To enable the above-mentioned applications, however, one remaining challenge must be met: packaging the SNSPDs so that the light can be efficiently coupled into the detectors. This step is difficult because of the small active area of the SNSPD and its low temperature operation.

To achieve such efficient coupling, we have designed an experimental setup to perform helium-immersed testing of SNSPDs inside a dewar. The major part of the setup is a probe in which are integrated a chip-holder, a fiber-focuser, three nanopositioners, a temperature sensor, and electrical connections. The fiber-focuser is used to shrink the spot-size of the light from a single-mode fiber down 5 μm, and the nanopositioners are used to accurately adjust the position of the spot in-situ three-dimensionally. The detector is directly connected with an SMA connector through wire bonding. Figure 1 shows some preliminary results, and further optimization is being performed.

Meanwhile, a more convenient, plug-in SNSPD system is being developed based on a closed-cycle, two-staged cryocooler that can reach 2.8 K (see Figure 2). Its main parts include a two-stage cold head, a compressor, a pump system, and a vacuum chamber. The main advantage of the cryocooler over the dewar is that it does not need liquid helium and is free to move. Therefore, this SNSPD system can facilitate many experiments in the field of quantum optics.

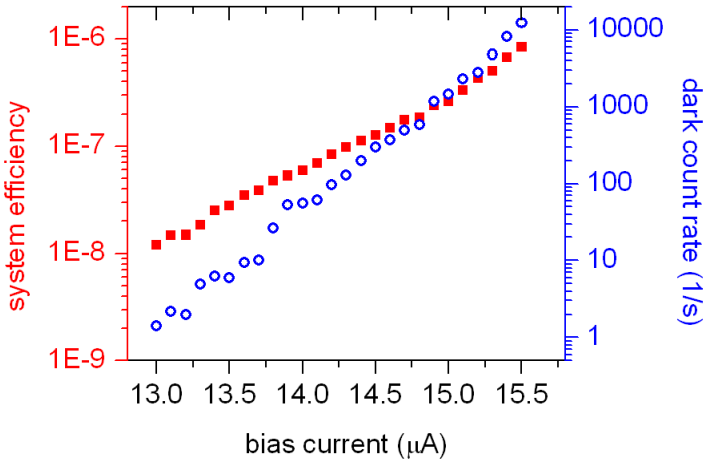

▲ Figure 1: System efficiency and dark count rate of a single-photon detector measured by helium-immersion testing.

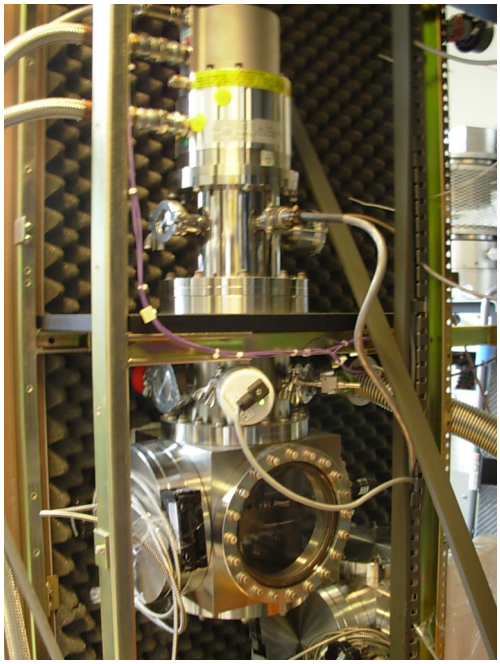

▲ Figure 2: The two-stage cryocooler for the testing of superconductive nanowire single-photon detectors.

Reference

[1] K.M. Rosfjord, J.K.W. Yang, E.A. Dauler, A.J. Kerman, V. Anant, B.M. Voronov, G.N. Gol'tsman, and K.K. Berggren, "Nanowire single-photon detector with an integrated optical cavity and anti-reflection coating," *Optics Express*, vol. 14, issue 2, pp. 527-534, Jan. 2006.

Trapping Ions with a Superconducting Ion Trap

Y. Ge, E. Dauler, J. Labaziewicz, S. Wang, I. Chuang, K.K. Berggren
Sponsorship: NSF Center for Ultracold Atoms, Japan Science and Technology Agency, MIT

We demonstrate an approach for fabricating a superconducting surface-electrode ion trap. Surface-electrode ion traps, while promising for large-scale quantum computation, have long been challenged by ion heating rates, which increase rapidly as trap length scales are reduced [1-3]. One promising approach to solve this problem is to fabricate trap electrodes from superconductors and to operate the ion trap chip at cryogenic temperatures.

The surface-electrode superconducting ion trap was fabricated from 140-nm-thick NbN on an insulating sapphire substrate. As Figure 1 shows, the ion trap has one RF, one ground, and four DC electrodes. Ions are trapped 100 μm above the surface in the center of the central ground electrode [4]. The NbN was deposited on R-plane sapphire using DC magnetron sputtering of a Niobium target in a 12% N_2 + 88% Ar gas mixture. Before deposition, the wafer was backside-coated with Niobium and the wafer was heated on an 800°C inconel block during the NbN deposition. The resulting ~140-nm-thick NbN film was superconducting at temperatures below T_c = 13K. In order to define the electrodes, optical lithography was performed using negative photoresist (NR9-3000) and this pattern was transferred into the 140-nm-thick NbN film using reactive-ion-etching with CF_4 and O_2. Finally, gold contact pads were defined by optical lithography using positive photoresist (S1813) and a liftoff process. To preserve superconductivity, all baking procedures were performed at or below 90°C.

The superconducting NbN ion trap successfully trapped single ions at temperatures sufficiently below its critical temperature, where the superconductivity could be maintained while applying the required trapping voltages. We measured the ion heating rates while operating the superconducting NbN ion trap at 6K. A single strontium ion was sideband-cooled to its quantum ground state motion, as shown in Figure 2. One 100-μm-size superconducting NbN ion trap showed an ion heating rate of 10~20 quanta, similar to low-resistivity, non-superconducting ion traps at cryogenic temperatures. When the temperature was above T_c, the NbN ion trap failed to trap ions due to the large resistivity change of the NbN RF electrode around T_c. In the future, superconducting traps with lower normal-state resistivity will be investigated in order to study how the electrode resistivity influences the ion heating rate.

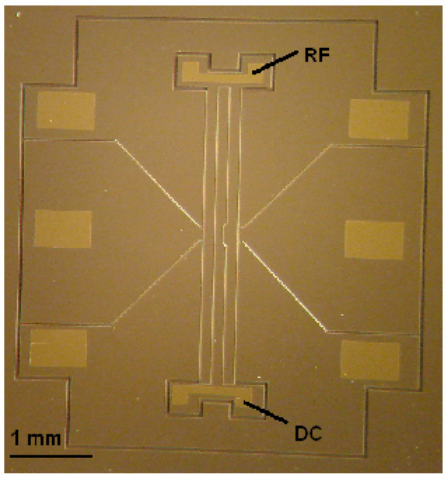

▲ Figure 1: Optical microscope photograph of a surface electrode NbN ion trap with gold contact pads. The ion trap consists of one RF, one ground, and four DC electrodes.

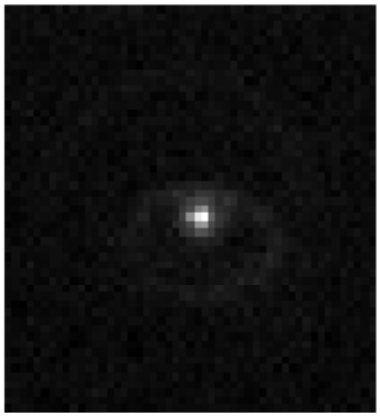

▲ Figure 2: A single strontium ion is trapped with the surface electrode NbN ion trap at 6K, sideband-cooled to its quantum ground state motion.

References

[1] D. Stick, W. K. Hensinger, S. Olmschenk, M.J. Madsen, K. Schwab, and C. Monroe, "Ion trap in a semiconductor chip," *Nature Physics*, vol. 2, pp. 36-39, Jan. 2006.
[2] L. Deslauriers, S. Olmschenk, D. Stick, W.K. Hensinger, J. Sterk, and C. Monroe, " Scaling and suppression of anomalous heating in ion traps," *Physical Review Letters*, vol. 97, p. 103007, Sept. 2006.
[3] S. Seidelin and J. Chiaverini, " Microfabricated surface-electrode ion trap for scalable quantum information processing," *Physical Review Letters*, vol. 96, p. 253003, June 2006.
[4] J. Labaziewcz, Y. Ge, P. Antohi, D. Leibrandt, K. Brown, and I.L. Chuang, " Suppression of heating rates in cryogenic surface-electrode ion traps," *Physical Review Letters*, vol. 100, p. 130001, 2008.

Guided-wave Devices for Holographic Video Display

D. Smalley, V.M. Bove, Jr., Q. Smithwick

Sponsorship: CELab, Digital Life, and Things That Think Research Consortia, Media Laboratory

We are developing a guided-wave optical modulator [1, 2] with 1-GHz composite bandwidth Surface Acoustic Wave (SAW) transducer arrays for use in video displays. This device is designed to diffract light horizontally and deflect it vertically through mode conversion by creating surface acoustic waves that interact with light trapped in waveguides on the surface of a lithium niobate substrate. To fabricate this modulator, we first mask a wafer of Z-cut lithium niobate with SiO_2 through a plasma-enhanced chemical vapor deposition (PECVD) process and then immerse it in heated benzoic acid and lithium benzoate to create single polarization waveguides. The waveguide is subsequently annealed to restore its acoustic properties. Finally, we pattern aluminum transducers onto the waveguides by conformal contact lithography employing a negative resist lift-off technique.

The goal of this work is to enable the inexpensive manufacturing of Scophony-architecture video displays [3] (both 2D and holographic video [4-5]) without the need for the horizontal scanning mirrors that typically limit the scalability of this technology.

Figure 1: A device undergoing testing.

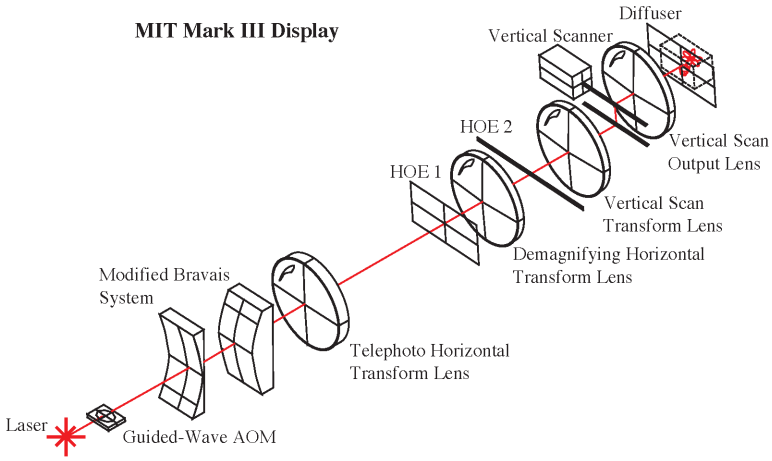

Figure 2: Architecture of our display system.

References

[1] C.S. Tsai, Q. Li, and C.L. Chang, "Guided-wave two-dimensional acousto-optic scanner using proton-exchanged lithium niobate waveguide," *Fiber and Integrated Optics*, vol. 17, pp. 57-166, 1998.

[2] D. Smalley, "Integrated-optic holovideo," Master's thesis, Massachusetts Institute of Technology, Cambridge MA, 2006.

[3] H.W. Lee, "The Scophony television receiver," *Nature*, vol. 142, pp. 59-62, July 1938.

[4] D.E. Smalley, Q.Y.J. Smithwick, and V.M. Bove, Jr., "Holographic video display based on guided-wave acousto-optic devices," *Proc. SPIE Practical Holography XXI*, vol. 6488, p. 64880L, 2007.

[5] W. Plesniak, M. Halle, V.M. Bove, Jr., J. Barabas, and R. Pappu, "Reconfigurable image projection (RIP) holograms," *Optical Engineering*, vol. 45, p. 115801, Nov. 2006.

Selective Epitaxial Growth of Ge for Photodiode Applications

M. Kim, O.O. Olubuyide, J.L. Hoyt

Sponsorship: DARPA, NSF Graduate Research Fellowship

We studied and optimized the growth parameters for selective epitaxial growth of Ge-on-Si for application of photodiodes operating at 1.55 μm [1]. Approximately 1 μm-thick, relaxed Ge was grown in exposed Si regions on oxide-patterned Si wafers. Germanium morphology and threading dislocation density were studied as functions of growth and processing conditions.

The morphology of the Ge films, especially faceting, becomes an issue when the Ge growth area is defined by vertical oxide walls, and a good hole-filling behavior is desired. Unlike the selective epitaxial growth of Si, where reducing the temperature reduces the {311} facet [2], selective Ge growth shows the opposite behavior and the {311} facet is reduced for increasing temperature. With the chamber pressure kept constant, GeH_4 partial pressure was increased to further increase the lateral growth of Ge and thus improve the hole-filling behavior (see Figure 1). At the optimized growth condition of 750°C and 10T, an RMS surface roughness of 1.3 nm was obtained for 10x10μm AFM scans.

A recent study reports aspect-ratio trapping of dislocations in Ge grown on Si in narrow regions [3]. In larger-dimension structures, it has also previously been shown that the Ge threading dislocation density can be reduced by annealing the film after Ge growth [4]. For Ge SEG, cyclic annealing is more effective in reducing dislocation density as the diode size shrinks, and an etch pit density of ~$2x10^6$ cm^{-2} has been reported for square Ge mesas of sizes >18μm [4]. We have investigated the reduction of threading dislocation density in cyclic annealed Ge-on-Si for feature sizes less than 10μm using cross-sectional and plan-view transmission electron microscopy (TEM) imaging. The threading dislocation densities that were observed here by TEM are higher than those reported in [4], but the trend of decreasing dislocation density with feature size continues for Ge growth areas with widths less than 10 μm (see Figure 2). Further optimizing the annealing condition should enable improvements in Ge-on-Si material quality obtained in features with dimension less than 5 μm.

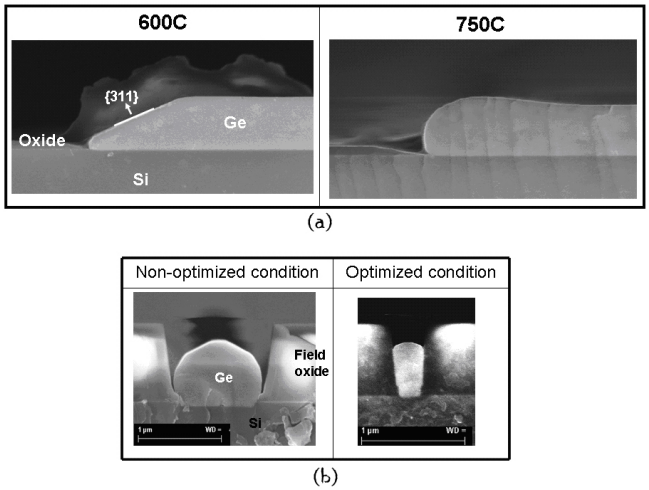

▲ Figure 1: (a) SEM images showing the reduction of Ge {311} faceting with the increase of temperature. (b) The optimized condition was used to grow Ge photodiode structures.

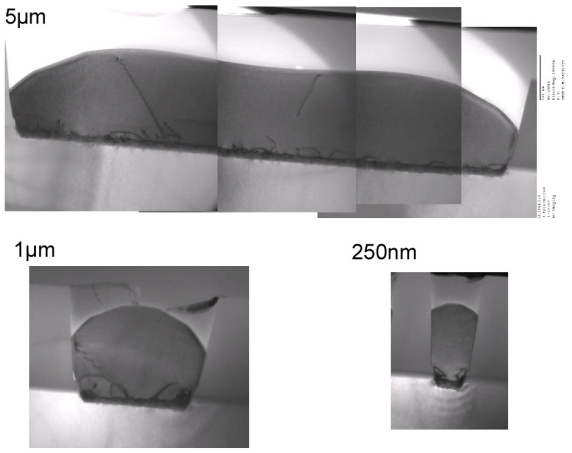

▲ Figure 2: Cross-sectional TEM images of SEG Ge structures with different widths. Ge film thickness is 0.8 μm. After growth the wafers were subjected to 4 cyclic anneals with minimum and maximum temperatures of 450 and 800°C. Dislocation density is significantly reduced for smaller features.

References

[1] F.X. Kärtner et al., "Photonic analog-to-digital conversion with electronic-photonic integrated circuits," in *Proc. SPIE*, vol. 6898, Feb. 2008, p. 689806.

[2] A. Talbot, J. Arcamone, C. Fellous, F. Deleglise, and D. Dutartre , "Investigation of facet formation in RTCVD Si/SiGe selective epitaxy," in *SiGe: Materials, Processing, and Devices*, D. Harame, Ed. New Jersey: The Electrochemical Society, Inc., 2004.

[3] J.-S. Park, J. Bai, M. Curtin, B. Adekore, M. Carroll, and A. Lochtefeld, "Defect reduction of selective Ge epitaxy in trenches on Si(001) substrates using aspect ratio trapping." *Applied Physics Letters*, vol. 90, Feb. 2007, p. 052113.

[4] H.-C. Luan, "Ge photodetectors for Si microphotonics," Ph.D. thesis, Massachusetts Institute of Technology, Cambridge, 2001.